Farah Christina Alimagham

Licenciada em Engenharia de Micro e Nanotecnologias

Assessment of a Microfluidic Intravenous Oxygen Generating Platform to Aid Acute Respiratory Failure

Dissertação para obtenção do Grau de Mestre em
Engenharia de Micro e Nanotecnologias

Orientador: Professor Doutor Babak Ziaie, Professor Catedrático, Purdue University, USA

Co-orientador: Professora Doutora Elvira Fortunato, Professora Catedrática, Faculdade de Ciências e Tecnologia da Universidade Nova de Lisboa, Portugal

Júri:

Presidente: Prof. Doutor Rodrigo Martins
Arguente: Prof. Doutor Hugo Águas
Vogal: Prof. Doutora Elvira Fortunato

FACULDADE DE CIÊNCIAS E TECNOLOGIA
UNIVERSIDADE NOVA DE LISBOA

September 2015

"Logic will get you from A to B.
Imagination will take you everywhere."

− Albert Einstein

Assessment of a Microfluidic Intravenous Oxygen Generating Platform to Aid Acute Respiratory Failure

ACKNOWLEDGEMENTS

First and foremost, I gratefully acknowledge the support and guidance of my supervisor, Dr. Babak Ziaie. He has given me relentless backing through the progress of my project and also groomed my graduate career by providing me with enriching opportunities.

I wish to thank my co-supervisor, Dr. Elvira Fortunato, for all her help support and for magnifying my interest in the world of micro and nanotechnologies from the very beginning.

A special thanks goes to Dr. Rodrigo Martins for all his time, encouragement and opportunities he has provided me throughout my studies.

I thank Manuel Ochoa for sharing his knowledge and expertise with me, for all the help in the lab, and for the brainstorming sessions that always lead to new and creative ideas. I also thank Albert Kim for all his advice and help in the lab whenever it was needed. In addition, I gratefully acknowledge the support of all the ZBML research group members for invaluable suggestions and assistance throughout my project and time at Purdue.

The National Science Foundation (NSF) is thanked for providing financial assistance for this research under grant EFRI-BioFlex #1240443.

All the staff and engineers at the Birck Nanotechnology Center of Purdue University are acknowledged for all their help and guidance.

I thank Daniel for the past five years of complete randomness, for understanding me at times that no one else could, for putting up with me on the good and bad days and most importantly for a true and forever-lasting friendship. I also thank Emanuel, for all the uplifting moments, wholehearted happiness and great friendship throughout the years. A massive thanks to Catarina for the wonderful person that she is, for understanding me and for being the best tissue engineering lab colleague I could have asked for. I also thank all my amazing friends and colleagues from Nova University of Lisbon that have been an important part of my academic life and made it an unforgettable one.

Words simply are not enough to express my gratefulness to my dear Amir, for being an unbelievable person, standing by my side all the way, giving me all the motivation and support in the world and having such a positive impact on my life. I would never have made it this far if it hadn't been for your endless patience, understanding and care.

Last but not the least, I would like to thank my family: my brothers Christopher and Kamran and my magnificent parents, Linda and Farshad, for their unconditional support, encouragement and belief throughout my education and entire life. For always being there for me and making me the person I am today.

ABSTRACT

Acute respiratory failure is associated with a high mortality rate, despite the advances in conventional treatments.

This work presents the development of a proof-of-concept device for assessing the viability of an oxygen-generating catheter, deployed intravenously, to temporarily sustain a patient who is suffering from acute respiratory failure. The assessment device mimics the interface between the catheter and bloodstream (deoxygenated water substitutes the blood), and consists of two parallel channels separated from each other by an oxygen-permeable membrane that simulates the catheter material. Several polydimethylsiloxane membranes with enhanced permeability were developed and tested on the device according to their permeation rates.

The highest permeation rate achieved was 3.6×10^{-7} cm^3/s (equivalent in-blood value) considering the device's surface area and applied pressure. However, the extrapolation of this value to a catheter with increased surface area demonstrated a predicted oxygen permeation rate of 1.6×10^{-3} cm^3/s.

Although the oxygen permeation rates achieved here do not yet reach the minimum required rate to sustain a patient with only 30 % of their lungs functional (1.6 cm^3/s O_2), it may be enhanced further by improving certain parameters such as material permeability, surface area and applied pressure.

The ability to administer oxygen or other gases directly into the bloodstream may portray a technique for short-term rescue of severely hypoxemic patients to increase whole body or at-risk organ oxygenation.

Keywords: Acute respiratory failure, oxygenation, intravenous oxygen delivery, PDMS membranes, microsystems

RESUMO

Apesar dos avanços nos tratamentos convencionais, a insuficiência respiratória aguda é uma condição associada a uma elevada taxa de mortalidade.

O presente trabalho apresenta o desenvolvimento de um dispositivo "prova-de-conceito" para avaliar a viabilidade de um cateter intravenoso, gerador de oxigénio, para sustentar temporariamente um paciente sofredor de insuficiência respiratória aguda.

O dispositivo simula a interface entre o cateter e a corrente sanguínea (onde água desoxigenada substitui o sangue) e consiste em dois canais separados um do outro por uma membrana permeável ao oxigénio que simula o material do cateter. Foram desenvolvidas várias membranas de polydimethylsiloxane, com permeabilidades ao oxigénio refinadas, e de seguida testadas no dispositivo, de acordo com a taxa de permeação de oxigénio que possibilitam. A maior taxa de permeação obtida foi de 3.6×10^{-7} cm^3/s (valor equivalente em sangue), tendo em conta a área superficial da membrana exposta no dispositivo e a pressão aplicada. A extrapolação deste valor, considerando um cateter com elevada área superficial, demonstra uma taxa de permeação de oxigénio de 1.6×10^{-3} cm^3/s.

Apesar das taxas de permeação de oxigénio obtidas neste trabalho serem ainda insuficientes para atingir o valor mínimo requerido (1.6 cm^3/s O_2) para sustentar um paciente com 30 % dos pulmões funcionais, poderão ser aumentadas melhorando certos parâmetros tais como a permeabilidade do material, a área superficial e a pressão aplicada.

A capacidade de administrar oxigénio ou outros gases diretamente para a corrente sanguínea poderá representar uma técnica de salvação de curto prazo para pacientes altamente hipoxémicas, para aumentar a oxigenação de corpo inteiro ou de órgãos em risco.

Termos Chave: Insuficiência respiratória aguda, oxigenação, administração intravenosa de oxigénio, membranas de PDMS, microssistemas

TABLE OF CONTENTS

LIST OF FIGURES

LIST OF TABLES

LIST OF SYMBOLS

Symbol	Definition	Unit
A	Membrane area	cm^2
P	Permeability	cm^3 (STP) cm cm^{-2} cm Hg^{-1} s^{-1}
d	Diameter	mm
ΔP	Pressure difference	mm Hg
PaO_2	Arterial partial pressure of oxygen	mm Hg
SaO_2	Arterial hemoglobin oxygen saturation	%
CaO_2	Oxygen concentration	%
pO_2	Partial pressure of oxygen	mm Hg
w/v	Weight/volume	%
p	Partial pressure of gas	mm Hg
δ	Membrane thickness	µm
υ	Volume of gas penetrating membrane	cm^3/s
n	Porosity	%

LIST OF ABBREVIATIONS

Abbreviation	Definition
3D	Three dimensional
Ar	Argon
ARDS	Acute Respiratory Distress Syndrome
ARF	Acute Respiratory Failure
CH_4	Methane
CO	Carbon Monoxide
CO_2	Carbon Dioxide
CPI	Carbonized Polyimide
DI	Deionized
DO	Dissolved Oxygen
H_2	Hydrogen
He	Helium
HCl	Hydrochloric Acid
Hgb	Hemoglobin
H_2O_2	Hydrogen Peroxide
H_2S	Hydrogen Sulfide
ID	Inner diameter
IPA	Isopropanol
KI	Potassium Iodide
$KMnO_4$	Potassium Permanganate
M_c	Molecular weight between crosslinks
MnO_2	Manganese Dioxide
MR	Mass ratio
N_2	Nitrogen
$NaHCO_3$	Sodium Bicarbonate
NP	Nanoparticle
O_2	Oxygen
OD	Outer diameter
PDMS	Polydimethylsiloxane
PI	Polyimide
ppm	Parts per million
PS	Polystyrene

rpm	Rotations per minute
SDS	Sodium Dodecyl Sulfate
SEM	Scanning electronic microscopy
Si	Silicon

CHAPTER 1. INTRODUCTION

1.1 Motivation

Acute respiratory failure (ARF) is one of the most common types of organ failure and is associated with a mortality rate of around 40%, despite the current advanced ventilator support and extracorporeal oxygenation [1]. From 2001 to 2009, the number of ARF-related hospitalizations in the US increased from one million to two million [2]. There are a number of causes that may lead to acute respiratory failure such as airway obstruction, injuries that impair or compromise the respiratory system (e.g.: injury to the spinal cord or brain), Acute Respiratory Distress Syndrome (ARDS) and stroke [3]. As a consequence, the lungs cannot release oxygen (O_2) (from the inhaled air) into the blood and in turn, the organs can't get enough O_2-rich blood to function. This prolonged O_2 deprivation can quickly lead to serious conditions such as brain damage, cardiac arrest and even death. In order to prevent this from happening, immediate medical attention is essential so that O_2 is provided as soon as possible [4].

Conventionally, O_2 deprivation is treated with inspired O_2, mechanical ventilation and intubation; however, these methods are often too complicated to implement rapidly under emergency situations and outside of a hospital setting and may not provide O_2 at a sufficiently high rate to sustain normal function of specific vital organs [5], [6]. In addition, in certain ARF situations the airway is blocked (due to inflammation or other obstructive reasons) preventing intubation and necessitating direct delivery of oxygen to the blood via intravenous O_2 delivery, which may temporarily rise venous and arterial O_2 tensions, thus enabling a safe window of time for definitive intervention, such as institution of extracorporeal life support or placement of a tracheal tube [6]. For example, a patient with difficulty breathing and maintaining sufficient oxygenation could avoid a hypoxemic crisis during a prolonged mechanical ventilation or intubation attempt. The shortcomings of the current technologies to aid acute respiratory failure motivates investigation into the potential of developing a safe, quick, and effective system for rapid oxygenation. This poses significant challenges, and to our knowledge, no such system exists to this day. Researchers have studied the possibility of directly injecting O_2 gas into the blood at different infusion rates; however, in vivo experiments revealed its ineffectiveness due to fatal pulmonary embolisms, cardiac irregularities, hypotension and death caused by the formation of O_2 bubbles at infusion rates higher than 0.2 to 1 mL/kg per minute (equivalent to 10 to 25% of measured O_2 consumption in dogs) and also due to the necessity of frequent pauses in infusion [7]. A more recent study has demonstrated impressive results in which animals are maintained alive for 10–15 minutes of complete asphyxia by the injection of lipidic O_2-filled microparticles (LOMs) into the vein that deliver O_2 to hypoxic blood [3]. The fabrication of the LOMs, however, is not easily scalable for mass production, and the overall amount of O_2 storage in the particles is suboptimal due to it being stored as a gas.

We have concentrated our efforts in assessing the viability of a straightforward, low cost, and scalable approach for delivering O_2 into the bloodstream without the risk of forming O_2 bubbles or hemolysis. The method, which we wish to assess, is schematized in Figure 1.1.

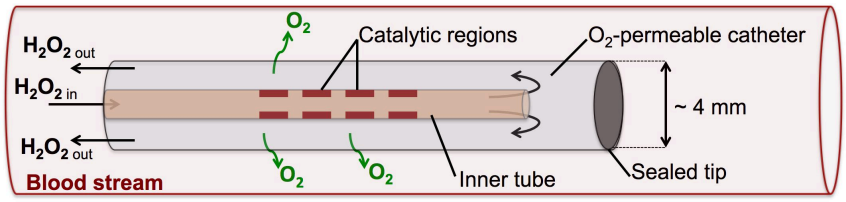

Figure 1.1. *Conceptual schematic of the proposed catheter approach for rapid delivery of oxygen to the blood.*

It consists of decomposing hydrogen peroxide (H_2O_2) into O_2 inside an end-sealed, custom catheter which is deployed intravenously; the H_2O_2 does not come in contact with live tissue, but enters the catheter through a concentric tube (on which it is possible to embed catalytic regions) and is decomposed into O_2 once in contact with the catalyst. The generated O_2 diffuses out into the bloodstream through the engineered O_2-permeable catheter material. In the present work, our aim is to evaluate the described approach in terms of its viability and O_2-supplying capacity regarding the possibility of providing a life-sustaining arterial O_2 saturation higher than 90% (pO_2 of 60 mm Hg). The amount of O_2 that a respiratory assist catheter positioned intravenously would need to add to an adult patient is 1.6 cm^3/s, considering that only 30% of the lung still functional. This amount corresponds to 50% of the basal O_2 requirements, as determined by calculated gas exchange requirements for an adult patient with various levels of pulmonary damage and residual functional lung [1]. In order to evaluate the described approach, a proof-of-concept device was developed according to the function principle depicted in Figure 1.2, where two parallel channels separated by an O_2-permeable membrane that will mimic the interface between the catheter and bloodstream. The O_2 generated in the bottom channel ("catheter") will diffuse through the membrane into the channel above ("bloodstream"), where its concentration will be measured.

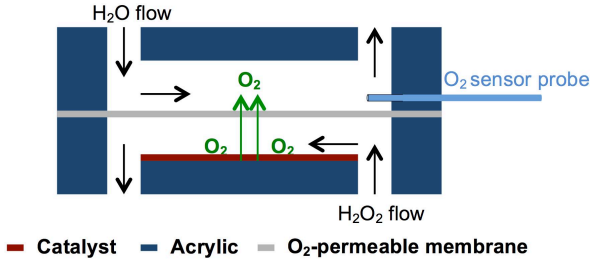

Figure 1.2. *Function principle of the proof-of-concept device to evaluate the approach.*

Several O_2-permeable membranes (catheter material) were developed using different permeability-enhancing techniques and assessed according to their O_2 diffusion capacity and O_2 permeability. Additionally, another section of the presented approach that was assessed was the possibility of

embedding catalytic regions on a tube that is used simultaneously as the H_2O_2 inlet and decomposing (into O_2) element.

Advancements in this field will contribute to the possibility of supplying O_2 directly into the bloodstream may represent a novel technique to increase O_2 delivery to the entire body or to specific vital organs for short-term rescue of profoundly hypoxemic patients.

The following section in this chapter describes the relevant theory behind this research. Chapter 2 discusses my chosen methodologies including the fabrication and characterization of the O_2 permeable membranes, the development and lab implementation of the bench-top test platform and also development of the inner tube of this approach. Chapter 3 sets out my results and discusses them, and Chapter 4 draws conclusions and describes relevant future work to be done in this approach.

1.2 Relevant Research

1.2.1 Physiological oxygenation

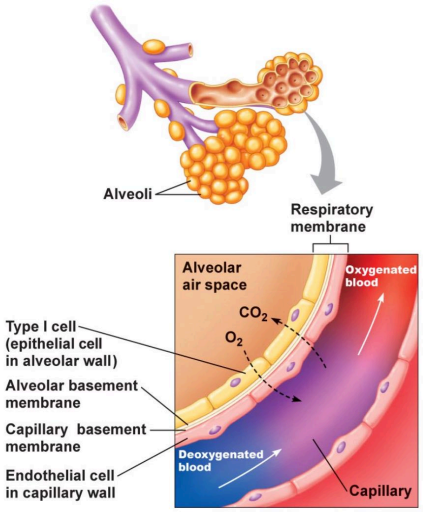

Figure 1.3. *Illustration on how O_2 and CO_2 go between alveolar air and blood across the respiratory membrane. [8]*

Oxygen plays a vital role in the breathing processes and in the metabolism of the living organisms and appropriate levels are vital to support cell respiration and survival. In the human body, O_2 diffuses through membranes and into red blood cells after inhalation into the lungs. Figure 1.3 illustrates how O_2 and carbon dioxide (CO_2) transit between alveolar air and blood across the respiratory membrane. The cells of the body consume an average of 250 mL O_2 per minute (4.17cm^3/s). A liter of blood can dissolve 200 cm^3 (mL) of O_2 gas, which is much more than water can dissolve (5.3 mL in a liter of air-saturated water at 30°C). The amount of O_2 that can be held by the water increases with decreasing temperature and salinity and decreases with pressure. Since O_2 is poorly soluble in water, without an adjunctive means of transport, it cannot be transported in blood in quantities sufficient to sustain life (the contribution of DO to the total is only 0.3 mL/dl or less than 1.5% of the total). The adjunct comes in the form of hemoglobin. O_2 can bind to hemoglobin at any of four active sites on each molecule of hemoglobin. Since there are four binding sites on the hemoglobin molecule the number of O_2 molecules on a hemoglobin molecule ranges from none to four. When four O_2 molecules are bound to the molecule, it is said to be 100% saturated. At 100% saturation 1 gram of hemoglobin carries 1.34 mL of O_2. The equation for the content of O_2 in arterial blood is as follows:

$$C_aO_2 = (SaO_2 \times Hgb \times 1.34) + (0.003 \times PaO_2) \qquad \textbf{(1.1)}$$

The term for SaO_2 (O_2 saturation) is expressed as a fraction of 1.0 rather than a percentage (i.e. 0.98 instead of 98%). Hemoglobin is entered in grams and PaO_2 (arterial partial pressure of oxygen) is in mmHg. The term 0.003, derived from O_2 solubility coefficients at different temperatures, assumes a normal body temperature of 37ºC and is expressed as mL O_2/dl/mmHg. The partial pressure (p) of a gas is the proportion of pressure contributed by an individual gas to the total pressure of a mixture of gases and is found by multiplying the fractional concentration of a gas in a mixture by the total pressure exerted by a gas mixture [8]. Although partial pressures of O_2 is 160 mm Hg, in the alveoli the pressure is 100 mm Hg, due to exchanges of gas between alveoli and capillaries, mixing of atmospheric air with air of anatomic dead spaces and saturation of alveoli air with water vapor. Deoxygenated blood entering the pulmonary capillaries has a pO_2 of 40 mm Hg. The O_2 diffuses down its concentration gradient and leaves at the same partial pressures as the O_2 in the alveoli (pO_2 = 100 mm Hg). The human body requires and regulates a very precise and specific balance of O_2 in the blood and normal levels in humans are considered 95-100%. If the level is below 90%, it is considered low resulting in hypoxemia. Blood O_2 levels below 80% may compromise organ function, such as the brain and heart, and should be promptly addressed. Continued low O_2 levels may lead to respiratory or cardiac arrest, where O_2 therapy may be used to assist in raising blood O_2 levels. Oxygenation occurs when O_2 molecules enter the tissues of the body. For example, blood is oxygenated in the lungs, where O_2 molecules travel from the air and into the blood. Oxygenation is commonly used to refer to medical O_2 saturation [9], [10].

When it comes to oxygen-related applications such as this one, finding an adequate way of storing and generating O_2 is vital. Methods of O_2 storage for subsequent use, span many approaches including high pressures in O_2 tanks, cryogenics, O_2-rich compounds and reaction mixtures, and chemical compounds that reversibly release O_2 upon heating or pressure change [11]. Hydrogen peroxide, a colorless liquid in its pure form, is a convenient O_2 storage medium due to its high O_2 composition and practical temporal stability at room temperature (up to a year for over-the-counter H_2O_2) and relatively easy production. The decomposition of H_2O_2 into O_2 can be induced by many means. The surface of manganese dioxide (MnO_2) is known to provide a particularly favorable environment to catalyze the decomposition through the following reaction [12]:

$$2\,H_2O_{2\,(aq)} \xrightarrow{MnO_{2(s)}} O_{2\,(g)} + 2H_2O_{(l)} \qquad \textbf{(1.2)}$$

1.2.2 Oxygen-permeable membranes: Why PDMS?

One of the main goals of this project is to choose a material with the ideal properties (i.e. biocompatibility, high oxygen permeability and simple processability) to be used in the final oxygenating system as the catheter material.

Polydimethylsiloxane (PDMS), has become the preferred material for lab on a chip (LOC) and microfluidic analysis platforms due to its properties: gas permeability, easy and low cost

processability, chemical stability, ability to be manipulated and biocompatibility [13]. It is a mineral-organic polymer, with a structure containing carbon and silicon, of the siloxane family (Figure 1.4).

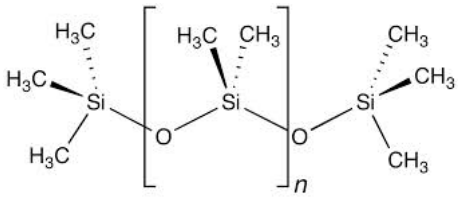

Figure 1.4. *Molecular structure of polydimethylsiloxane. [14]*

PDMS permeability has been extensively used to add new features and characteristics to microfluidic devices and it has been used to move fluids inside micro channels to obtain accurate control of the liquid and complete filling of the device. By employing this mechanism, it is possible to create a number of devices that avoid any sort of contamination of external material, since a thin membrane of PDMS acts as a barrier towards reagents and/or biological species during handling. Additionally, microfluidic bioreactor systems use PDMS permeability to ensure gas diffusion inside the reaction chamber for cell culturing applications. In this work, taking advantage of PDMS permeability is essential since our goal is to test an intravenous O_2-generating and supplying catheter, in which the generated O_2 permeates through the catheter material into the bloodstream. For these tests, it is necessary to obtain a thin PDMS membrane with tuned permeability so that it diffuses O_2 in a controlled way. Several successful investigations on enhancing gas perfusion, and thus PDMS permeability, have been performed. It has been shown by [15] that it is possible to greatly increase the permeation of gas molecules through PDMS membranes by varying PDMS composition (i.e. mixing ratio between oligomers and curing agent), which strongly influences the chemical and mechanical properties of the elastomer. Manipulating the pore size of PDMS is another permeability-enhancing technique that can be done by several methods. Kexin Jiao et al. [16] developed porous PDMS membranes that can selectively diffuse elements of different sizes by embedding micron sized $NaHCO_3$ particles in PDMS thin films. The membranes are then immersed in concentrated hydrochloric acid (HCl) to generate pores by evolution of CO_2 gas from the reaction between $NaHCO_3$ and HCl. A more simple way of fabricating microporous PDMS has been described by Juyue Chen et al. [17] and involves evaporating water from an emulsion of PDMS pre-polymer and water microbubbles. The high flexibility of the silicon-oxygen (Si-O) chains in silicones provides "openings", which are essentially free volumes that allow gas diffusion inside the network. Free volumes are frequently named "holes" and they are thermally generated and disappear with the movement of polymer chains. Gas molecule diffusion in rubber membranes is a process in which the gas molecules migrate from "hole" to "hole". The rate at which a gas or vapor passes through a polymer consists of three different permeation mechanisms, depicted in Figure 1.5: (a) absorption of the permeating species at the polymer/gas interface into the polymer; (b) diffusion through the polymeric membrane, and finally (c) desorption (also considered evaporation) of the permeating

species from the polymer surface and removal. The rate of permeation is a specific function of a given gas and rubber and it depends on both solubility and the diffusion rate. In most of applications, permeability of a membrane is used to characterize the rate of permeation and is usually calculated by the following equation:

$$P = \frac{\upsilon\delta}{At(p_1 - p_0)} \qquad \textbf{(1.3)}$$

where, P is the permeability for a given gas in a given membrane, υ is the volume of gas which penetrates through the membrane, δ is the thickness of membrane, A is the area of membrane, t is time, p_1 is the partial pressure of the gas on the higher pressure side of the membrane, and p_0 is the partial pressure of the gas on the lower pressure side of the membrane.

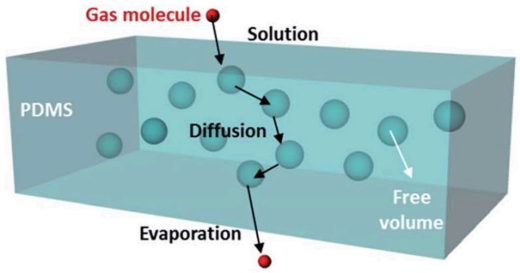

Figure 1.5. *3D scheme depicting the gas diffusion mechanism in a PDMS membrane. [15]*

In general, permeability of a polymer for a gas mixture increases with decreasing size and increasing solubility (or condensability) of the gas. The relative permeability of a gas is given below in order of decreasing gas permeability as:

$$H_2 > He > H_2S > CO_2 > O_2 > Ar > CO > CH_4 > N_2$$

The O_2 permeability in PDMS is significantly higher than in other polymers. Table 1.1 indicates O_2 permeabilities in various common polymer membranes.

Table 1.1. *O_2 permeabilities in various polymers [18].*

Polymer	**O_2 Permeability** $\times 10^9$ $[cm^3\,(RTP)\cdot cm\cdot s^{-1}\cdot cm^{-2}\cdot cm\,Hg^{-1}]$
PDMS	60
BPA polycarbonate	0.16
Polystyrene (PS)	0.12
Cellulose acetate	0.08

In our work, we attempt to enhance the permeability of PDMS membranes by using the previously mentioned techniques, namely varying the crosslink ratio of the PDMS, embedding $NaHCO_3$ particles to form pores (as well as a combination of these two) and a modified version (in film form) of the water-in-PDMS emulsion technique to form micropores. Also, we will use a combination of the first two techniques. These films will then be tested on the developed test platform and characterized in order to evaluate their performance for the desired application [19], [20], [21].

CHAPTER 2. MATERIALS AND METHODS

2.1 Oxygen-permeable membrane development and characterization

Several PDMS membranes were developed using three different permeability-enhancing techniques similar to what has been described in the literature. These techniques included: (A) increasing PDMS base-crosslinker ratio [15], (B) embedding $NaHCO_3$ particles in PDMS to generate porous membranes [16] and (C) creating a water-in-PDMS emulsion concentrations to generate microporous in-bulk PDMS [17]. The modifications we made to these techniques were combining the first two techniques (A and B) to develop macroporous PDMS membranes and using the water-in-PDMS emulsion technique (C) to develop microporous PDMS membranes (as opposed to in-bulk form described in literature).

2.1.1 Macroporous PDMS membrane development

Macroporous PDMS membranes were prepared using a combination of the base-crosslinker ratio variation and $NaHCO_3$ particle embedment techniques. The membranes were prepared mixing polymer base and the curing agent (Sylgard 184, Dow Corning, Midland, MI) with different weight ratios (10:1, 15:1, and 20:1)[a]. Powdered $NaHCO_3$ (AR. ACS Grade, 99.7-100.3 %, Mallinckrodt, St. Louis, MO, USA) at different concentrations (0, 10, 15, 20 and 30%) was manually grinded using a mortar and pestle and mixed in the pre-polymerized PDMS at different ratios. A spin-coater (6800 Spin Coater, Specialty Coating Systems, Indianapolis, IN, USA) was used to control the thickness of the PDMS membrane using defined spinning rates with thicknesses in the range of 70-220 μm. Table 2.1 shows the parameters used to develop the membranes. The membranes were spin-coated for 30 seconds onto silicon wafers which were first silanized using a drop of trichloro(3,3,3-trifluoropropyl)-silane (97%, Sigma-Aldrich, Inc., St. Louis, MO, USA) in vacuum to prevent the PDMS from adhering to it after curing. The resulting membranes were cured in an oven (Single-Wall Transite Oven, BlueM Electric Company, Blue Island, IL, USA) at 75 ^{o}C, the optimal cross-linking temperature, resulting in membranes with the highest gas permeation compared to those cross-linked at RT or above 100 ^{o}C, according to K. Berean et al. [23]. Once cured, the membranes with higher base-crosslinker ratio than the standard (10:1) were first placed in a solvent, Hexane (anhydrous, 95%, Sigma-Aldrich, Inc., St. Louis, MO, USA), overnight in order to induce membrane swelling and dilation so that the uncrosslinked regions are removed, leading to a higher volume of open spaces within the membrane. The membranes were then placed first in Acetone (J.T.Baker, Avantor Performance Materials, Inc., Center Valley, PA, USA) and then Isopropanol (IPA) (J.T.Baker, Avantor Performance Materials, Inc., Center Valley, PA, USA) and immersed in ultrasonic for one

[a] A MR equal to 10:1 is the standard composition (suggested by the producer) representing the adequate balance between the two components in order to obtain the minimum amount of unreacted species in the cross-

hour in each in order to shrink back to their original size. The membranes containing any percentage of $NaHCO_3$ particles were then immersed in 10 % HCl (36.5-38.0 %, J.T.Baker, Avantor Performance Materials Inc., Center Valley, PA, USA) for 1-3 days in order to dissolve away all the $NaHCO_3$, leaving behind voids within the membranes. Bubbles were observed during this process, indicating that CO_2 was released from the reaction between the HCl and the embedded $NaHCO_3$. After removal from HCl, the membranes were washed thoroughly with water and ethanol and air-dried.

Table 2.1. *Macroporous PDMS membrane specifications.*

Membrane	Spin-coating speed (rpm)	$NaHCO_3$ (%)	PDMS base-crosslinker ratio
1.1	1000	0	15:1
1.2	500	10	15:1
1.3	500	20	15:1
1.4	500	30	15:1
1.5	1600	20	20:1
1.6	1600	15	20:1
1.7	1300	20	10:1
1.8	1300	30	10:1
1.9	1000	20	15:1
1.10	1000	30	15:1

2.1.2 Microporous PDMS membrane development

The technique used to develop microporous PDMS membranes was the water-in-PDMS emulsion technique. PDMS was mixed with the standard mass ratio of base-crossliker (10:1). A sodium dodecyl sulfate (SDS) (Molecular Biology Grade, > 99 %, Research Products International Corp., Mt. Prospect, IL, USA) was prepared with a mass ratio of SDS to DI water of 1:100. The PDMS pre-polymer and water (with 1% SDS) were manually blended together at different volume percentages (20 and 30 %) until a uniform emulsion (opaque) was formed. The water-in-PDMS emulsion was then spin-coated for 30 seconds at different speeds to control thickness. Table 2.2 represents the spin-coating and water percentages used in the membrane development. The mixture was first place in the oven for 15 minutes at 75 ^{o}C until the pre-polymer is partially cured with the water microdroplets inside. Then they were immediately transferred to a hotplate at a higher temperature of 120 ^{o}C so that the water trapped in the PDMS membrane evaporates, leaving behind numerous pores within the matrix.

Table 2.2. *Microporous PDMS membrane specifications.*

Membrane	Spin-coating speed (rpm)	Water (%)
2.1	500	20
2.2	500	20
2.3	1000	30

Light microscopy images were obtained for the functional porous membranes developed using the $NaHCO_3$ technique and one of the films developed by developed by water-in-PDMS emulsion using a High performance Microscope (MicroZoomII S-450, Bausch & Lomb Inc., Bridgewater, New Jersey, USA). For all the microporous membranes developed by water-in-PDMS emulsion, SEM images were obtained on a Field-emission Scanning Electron Microscope (FE-SEM) (S-4800, Hitachi, Japan). The membranes were mounted on a carbon tape affixed to an aluminum stub and loaded in the SEM. The use of image analysis software, ImageJ (version 1.48, NIH, USA), was used to quantify the percent porosity and pore size of the functional membranes.

2.1.3 Permeability characterization

A custom made permeation measuring platform was developed in order to characterize membrane permeability of both microporous membranes (20 % and 30 % water) and compare them to the known value of non-porous PDMS. The several components that constitute the platform are schematized in Figure 2.1.

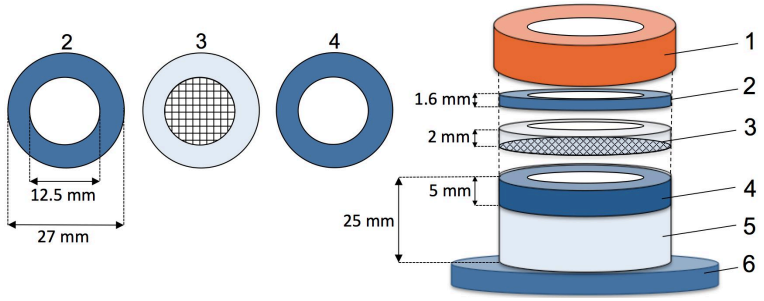

Figure 2.1. *Permeability measuring device and its components.*

This system is based on the permeability equation (eq. 1.3). Accordingly, if the values of the membrane thickness and exposed area are known, then, by applying a constant flow-rate and measuring the pressure difference across the membrane once it has stabilized, we are able to determine the permeability coefficient of the developed membranes [13]. The base of the permeation cell consisted of a conical test tube (50 mL, Falcon, Fisher Scientific, Inc., Waltham, MA USA) with the end cut off and bonded with Epoxy Adhesive (Devcon Adhesives & Sealants, Danvers, MA, USA). A circular acrylic ring (4) was sealed inside the tube with glue. In order to keep the films from expanding (i.e. a constant permeation area), aluminum screening (New york wire, Grand Island, NY, USA) was embedded in a PDMS ring (3). An additional acrylic ring (2) is used to press the PDMS ring firmly against the acrylic ring bellow using the tube's screw-on lid (1) so that the platform is air-sealed. For the measurements, the PDMS membranes were mounted between rings 3 and 4 with an exposed area of 12.5 mm^2. The apparatus used for measuring permeation rates for O_2 in the PDMS membranes is depicted schematically in Figure 2.2. The entire setup is filled with 100% O_2 gas. Initially, O_2 was flushed through A and out first through B and C simultaneously. Then, a 60 mL syringe was attached to B and C is sealed off with a luer plug so that the syringe was left to fill. Once

the system is filled with 100 % O_2, the syringe is placed on the single syringe pump and a constant flow-rate is applied (between 10 and 30 µL/min).

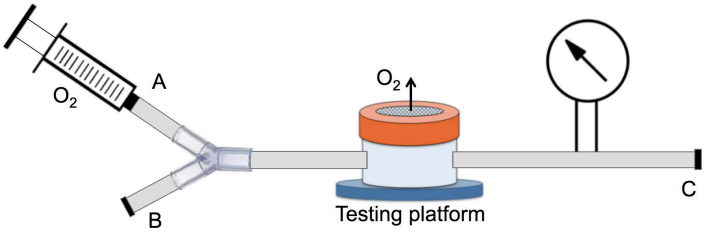

Figure 2.2. *Permeability measuring setup.*

The pressure was continuously monitored on the High Accuracy Digital Pressure Gauge (DPG4000 Series, OMEGA Engineering Inc., Stamford, CT, USA) until stabilized. At steady state condition, gas permeability was calculated using eq. 1.3. Leakage of the device was tested before each use. In order to do this, a sacrificial membrane was mounted on the platform and the entire setup (including all luer connections and endings) was submerged in water and pressures up to 600 mm Hg were applied to the syringe. If no bubbles were noticed, the device was ready to use. A normal PDMS membrane was first tested on this setup in order to determine its accuracy. All measurements were carried out at room temperature, 21 ºC.

In order to analyze the deflection capacity of a standard PDMS membrane to increasing pressures and evaluate the amount of pressure it is able to withstand, the same platform and setup as the permeability test was used, except for this time, the aluminum screening embedded in a PDMS ring was replaced with a PDMS ring without the screening to enable deflection of the membrane. Increasing pressures were applied manually to the setup (starting from 10 mmHg to 820 mmHg) using a 60 mL syringe. Images of the membranes were captured at the varying pressures.

2.2 Proof-of-concept device

2.2.1 Fabrication

A proof-of-concept device that mimics the catheter-bloodstream interface was developed to test the viability of our approach, and therefore, the O_2 diffusing capacity of several PDMS membranes with enhanced O_2-permeability. Figure 2.3 represents the several components that constitute the device. The device was fabricated by stacking and sealing together (using screws) intercalated layers of PDMS and acrylic. The PDMS layers (2 and 5) act as a sealant between layers while 2 also provides a firm fitting for the liquid inlet/outlet elbow fluid-connectors (Value Plastics Inc., Nordson Company Fort Collins, CO) that are inserted through the top acrylic layer (1). The acrylic layers (1, 3, 4 and 6) provide the device with rigidity so that all layers can be clamped together using screws and knots in order to prevent any leakages out of the channels. First, PDMS was mixed according to manufacturer specifications and poured into a Petri dish. After curing for 4 hours at 75 ºC in the oven, the PDMS was demolded. PDMS and acrylic layers were cut into the desired shapes using a

commercial 10.6 µm pre-aligned CO_2 laser engraver (PLS6MW, Universal Laser Systems Inc., Scottsdale, AZ, USA); the CO_2 laser was used with a maximum power of 75 W and maximum linear speed of 4 m/s.

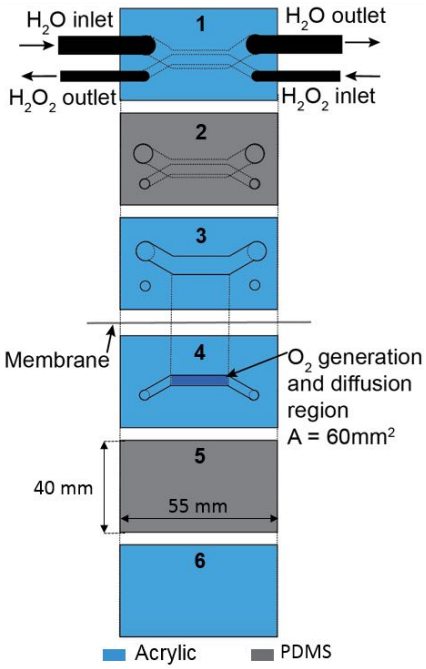

Figure 2.3. *Schematic of the several componentes that constitute the testing device.*

The shape designs were made using Coral draw software (CorelDRAW Graphics Suite X6, Corel Corporation) and transferred to the PLS6MW Laser Viewer software for setting adjustments and operating the laser. The laser settings used for each of the materials and respective thicknesses are shown in Table A.1, Appendix A. Layers 1, 4 and 6 have a thickness of 1.6 mm; layers 2 and 3 are 5 mm thick and layer 5 is 3 mm thick. The two innermost acrylic layers (3 and 4) contain the two laser-machined parallel channels that mimic (in dimension and applied pressure) the interface between the catheter (lower channel) and bloodstream (upper channel) once separated by an O_2-permeable membrane. The upper channel was made to hold the same volume as the human basilic vein (typically 5 mm diameter, holding 2 mL in a 1 cm section), with dimensions 3×28×1.6 mm^3, while the lower channel has an exposed surface area of 60 mm^2. A 1 mm-thick strip of PDMS loaded with the MnO_2 microparticles (≥ 99 %, Sigma Aldrich, St. Louis, MO, USA), with the particles exposed at the surface, made by mixing the MnO_2 particles in uncured PMDS, pouring it into a petri dish and curing it at 75 ºC. Once cured, it is demolded and cut into channel-size strips with a razor blade so that it fits into the bottom of the lower channel.

2.2.2 Lab implementation

In this section, the lab setup to implement the device for membrane assessment is described in detail. Here, a controlled flow of de-oxygenated (bubbled with nitrogen gas), de-ionized water is pumped through the upper channel in the opposite direction of H_2O_2 flow that is pumped through the

channel bellow (channels are separated by a membrane). Water was used in the tests since it is easier to handle on a daily basis than is blood. Water data, however, can be accurately converted to data obtained with blood by multiplying water results by a factor of 5, based on blood solubility and viscosity compared to water [1], [24]. The H_2O_2 (30 %, J.T.Baker, Avantor Performance Materials, Inc., Center Valley, PA, USA) at 15 % concentration is pumped through the lower channel at a constant flow, where it is decomposed into O_2 by the chemical catalyst, MnO_2 microparticles, within the channel. The amount of O_2 that diffuses through the membrane and is released into the deoxygenated water (upper channel) was quantified using an optical O_2 sensor (Neofox Oxygen Sensor, Ocean Optics Inc., Dunedin, FL, USA). Figure 2.4 reveals the setup used to implement the device. Appendix B shows a real image of the lab implementation of the testing device.

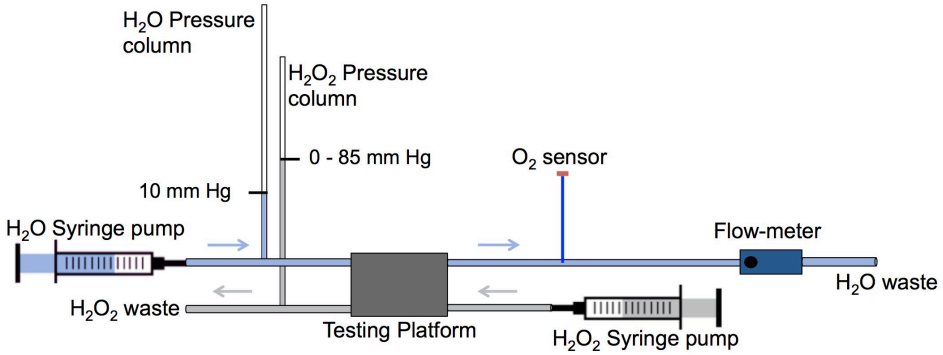

Figure 2.4. *Laboratory setup for implementing the fabricated testing device.*

Initially, a given membrane was carefully mounted on the unassembled device so that it separates the two channels. The device was then assembled and clamped. Before running any tests, the device and membrane were checked for leakages by flowing a dyed solution (5% food coloring in DI water) through the lower channel. For any dyed water that passed through into the upper channel indicates a leakage in the device or a torn/faulty membrane to be discarded. In order to have a controlled flow-rate in both channels, two 140 mL syringes (Covidien Ltd., Suwanee, GA, USA), mounted on a double syringe pump (NE-4000, New Era Pump Systems Inc., Farmingdale, NY, USA), were connected to the upper channel inlet and a 60 mL syringe (BD, Franklin Lakes, NJ, USA), mounted on a single syringe pump (NE-1000, New Era Pump Systems Inc., Farmingdale, NY, USA) was connected to the lower channel inlet. The flow-rates in the upper (H_2O) and lower (H_2O_2) channels were 1 mL/min and 0.5 mL/min respectively. Both fluids were set to flow through Medical Grade Teflon tubes from the syringe pump, past the pressure column, and through the O_2-generating device. The Teflon tube carrying the deoxygenated water had an inner diameter of 5 mm (approximate diameter of the basilic vein). Pressure columns were used to induce pressure in both channels. In the water channel, the pressure was kept constant at 10 mm Hg (hydrostatic pressure of the basilic vein) while the pressure in the H_2O_2 channel was gradually increased from 0 to 85 mm Hg, meaning that the pressure difference, ΔP, across a given membrane varied between -10 and 75 mm Hg. A light

microscope was used to verify the appearance of bubbles in the device during the tests. The O_2 sensor was calibrated using the standard two-point calibration described in the Installation and Operation Manual. A flow meter (RMA Series, Dwyer Instruments, Inc, Mich. City, IN, USA) was used at the end of the water channel in order to precisely control the flow rate in the H_2O channel. The sensor probe was then inserted into the water tube immediately after the O_2-generating platform and the concentration of O_2 inside the channel was measured with increasing ΔP across the channels during a given period of time. The data is acquired on its specified operating software (NeoFox Viewer, version 2.4). The acquired water data was accurately converted to blood data and an extrapolation was to determine the values that would be obtained for increased surface areas and pressure gradients.

2.3 Development of the MnO_2-embedded Polyimide tube

Figure 2.5 depicts the several steps taken to embed MnO_2 NPs in the polyimide (PI) tube wall.

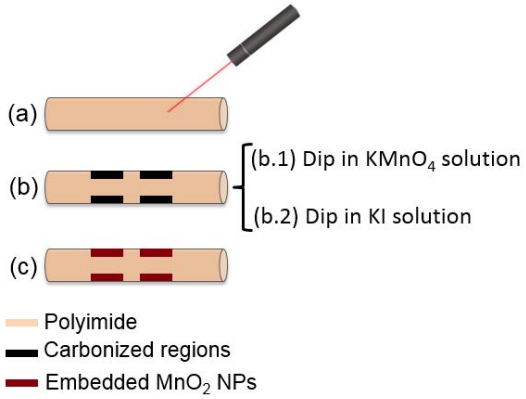

Figure 2.5. *Scheme depicting the procedure for embedding MnO_2 nanoparticles in a PI tube. (a) Carbonization of tube by laser-machining; (b) embedment of MnO_2 nanoparticles in; (c) PI tube with embedded MnO_2 nanoparticles.*

Select regions of the external wall of a PI tube (triple wall, Translucent Amber, Small Parts, Logansport, IN, USA) with 2 mm ID and 2.2 mm OD, were carbonized by controlled laser ablation using the CO_2 laser cutter. The PLS6MW Laser's rotary fixture accessory was used, providing the ability to engrave cylindrical objects. In order to place the polyimide tube on the rotator fixture, an aluminum wire with a similar ID as the tube was threaded through and fixed inside a conical test tube with a rectangular opening cut into the wall so the tube is exposed. The test tube was then fixed into the rotator fixture. The laser parameters used on the tube are included in Table A.1 – Appendix A. The carbonized residues provide a high surface area, allowing the embedment of MnO_2 nanoparticles. The MnO_2 particles were synthesized according to the following chemical reaction:

$$KMnO_{4(aq)} + KI_{(aq)} \rightarrow MnO_{2(s)} + KIO_{3(aq)} \qquad \textbf{(2.1)}$$

A 20 mL solution of 5 % w/v Potassium permanganate ($KMnO_4$) (powder, 97 %, Sigma-Aldrich, St. Louis, MO, USA) and a 20 mL solution of 5 % w/v Potassium Iodide (KI) (BioXtra, ≥ 99.0 %, Sigma-Aldrich, St. Louis, MO, USA) were prepared. The polyimide tube with carbonized regions was

first dipped into the $KMnO_4$ solution and then into the KI solution. The MnO_2 nanoparticles were synthesized *in situ*, embedded into the carbonized polyimide (CPI) tube. A 1 mL droplet of 15 % H_2O_2 was then placed on the tube using a disposable pipette in order to prompt the generation of O_2 through its decomposition by the MnO_2 nanoparticles.

CHAPTER 3. RESULTS AND DISCUSSION

We engineered a bench-top testing device to mimic the interface between the idealized custom catheter and the bloodstream. Several PDMS membranes with enhanced oxygen permeability were developed to mimic the catheter material of the final system and tested on the device regarding the oxygen permeation rate they enable. The oxygen generated within the channel of the device that mimics the catheter permeates into the channel that mimics the bloodstream and is measured by means of an oxygen sensor.

3.1 Oxygen-permeable membranes

The oxygen-permeable membranes that were developed based on the combination of the increased base-crosslinker ratio and $NaHCO_3$ embedment techniques as well as the water-in-PDMS emulsion technique and their corresponding parameters and functionality are shown in tables 3.1 and 3.2 respectively. As previously mentioned, before testing each membrane, they were first checked for leakages and other defects. The functional membranes (marked with ✓) were tested on the platform, while the membranes containing defects (marked with ×) were discarded.

Table 3.1. *Parameters of the macroporous membranes developed using $NaHCO_3$ and varying crosslink ratios.*

Membrane	Spin-coating speed (rpm)	Thickness (µm)	$NaHCO_3$ (%)	PDMS base-crosslinker ratio	Functionality
1.1	1000	100	0	15:1	✓
1.2	500	220	10	15:1	✓
1.3	500	220	20	15:1	✓
1.4	500	220	30	15:1	✓
1.5	1600	---	20	20:1	×
1.6	1600	---	15	20:1	×
1.7	1300	70	20	10:1	×
1.8	1300	---	30	10:1	×
1.9	1000	120	20	15:1	×
1.10	1000	---	30	15:1	×

Table 3.2. *Parameters of the microporous membranes developed using water-in-PDMS emulsion.*

Membrane	Spin-coating speed (rpm)	Thickness (µm)	Water-in-PDMS (%)	Functionality
2.1	500	200	20	✓
2.2	1000	70	20	✓
2.3	1000	90	30	✓

Regarding the macroporous membranes (Table 3.1), membranes 1.1 to 1.4 (corresponding to 0, 10, 20 and 30 % $NaHCO_3$ and 15:1 PDMS base-crossliker ratio), didn't show any defects or leakages during the leakage test and were therefore eligible for testing on the testing platform. On the other hand, membranes 1.5 to 1.8 and membrane 1.10 revealed to be too brittle and sticky for handling and were torn immediately upon removal from the HCl bath. The brittleness and stickiness of these films may be associated with simultaneous embedment of relatively high $NaHCO_3$ particle concentrations and high base-crosslinker ratios as well as their decreased thicknesses (for higher rotation speeds).

According to literature [15], the elastic modulus of free-standing PDMS membranes increases with the amount of crosslinker since a tighter network is formed. Accordingly, lower than suggested quantities of crosslinker could lead to a lower crosslinking density. Therefore when using PDMS base-crosslinker ratios much higher than suggested (10:1), the high disparity between pre-polymer and curing agent leads to a highly sticky and not manageable PDMS membrane. Even though literature suggests that a base-crosslinker ratio of 20:1 is perfectly manageable and results in a higher O_2 permeability, the addition of porogens, such as $NaHCO_3$ particles (in this case), did not allow for manageable membranes below a certain thickness. Membrane 1.9 (20 % $NaHCO_3$ and 15:1 PDMS base-crossliker ratio) showed favorable testing properties at first sight, as it was easy to handle and showed no signs of leakage. However, once it was setup on the device and a pressure gradient of 12 mm Hg across the membrane was achieved, signs of leakage were detected. A possible reason for the occurrence of leakages in this membrane is discussed and referred to in the next few paragraphs while discussing the porous membrane morphology.

For the reasons mentioned above, membranes 1.5 to 1.10 were discarded and focus was given to membranes 1.1 to 1.4 for the device tests.

Concerning the microporous membranes (Table 3.2), membranes 2.1 to 2.3 (corresponding to 20 % water in PDMS, spin-coated at 500 and 100 rpm, and 30 % water in PDMS, spin-coated 1000 rpm), there were no signs of leakage or brittleness, making them all good candidates for testing on the device.

Figure 3.1 shows light microscope images of the functional macroporous PDMS membranes (1.1 to 1.4), developed by $NaHCO_3$ particle embedment and one microporous PDMS membrane (2.1), developed by water-in-PDMS emulsion, for pore-size comparison. Images (a), (b) and (c) of figure 3.1 reveal a significant number of pores/voids within the membrane, that are possible to observe given the PDMS membrane transparency. The red circles outline the pores that are larger in dimension while the blue circles outline the pores that are smaller. The measured pore-sizes of these membranes range between 20 and 250 μm, representing a high non-uniformity, which may be explained primarily by the non-uniformity of the $NaHCO_3$ particles used in their development. Another contributing factor to the non-uniform pore shapes and sizes may be caused by the acid (HCl) treatment used to dissolve and wash away the $NaHCO_3$ particles during their development. The reaction between the $NaHCO_3$ particles and HCl released CO_2 gas, which contributed to the generation and expansion of the pores.

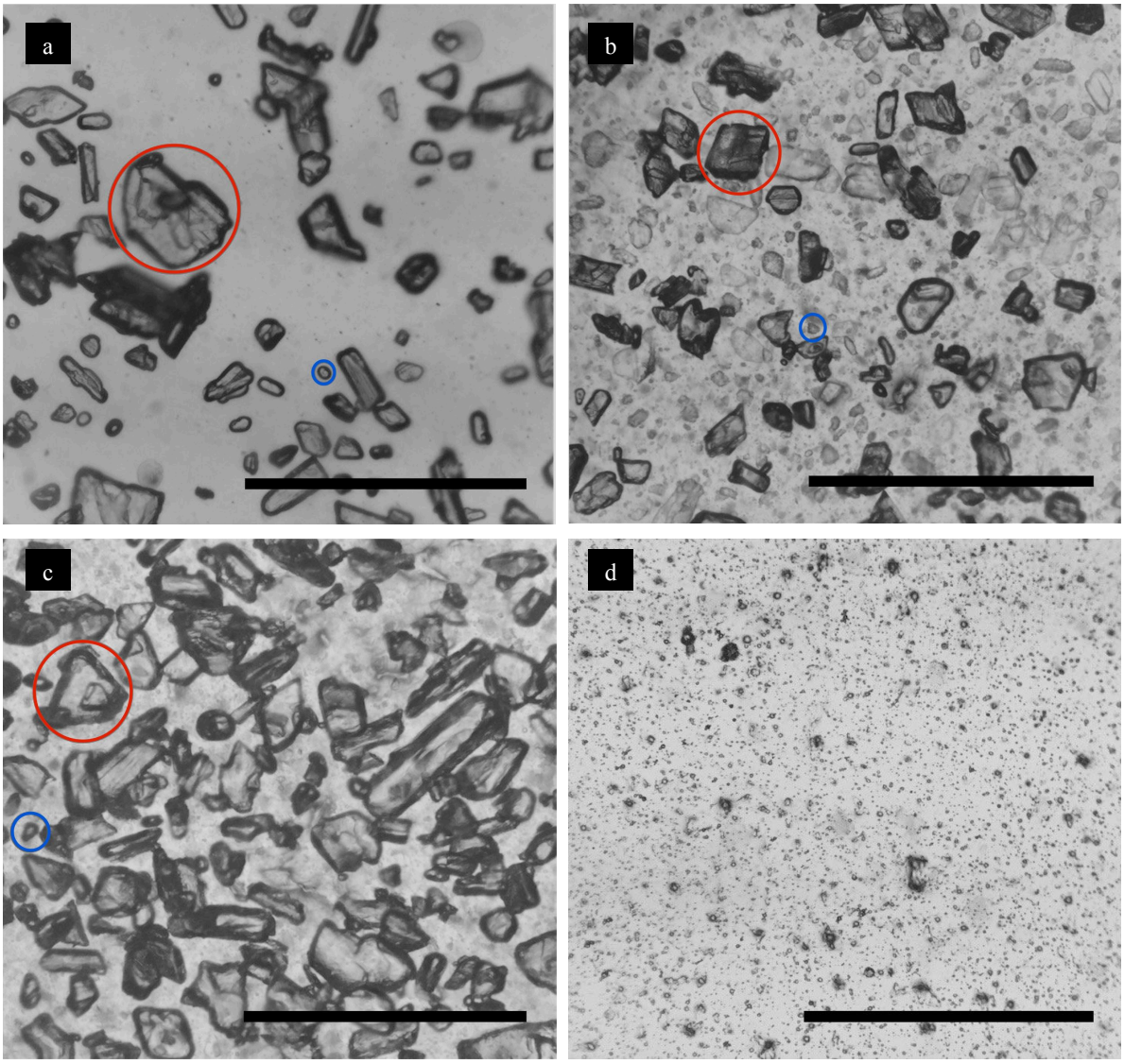

Figure 3.1. *Light microscope images showing the pores of the PDMS membranes prepared. (a) Membrane 1.2 (10 % $NaHCO_3$); (b) Membrane 1.3 (20 % $NaHCO_3$); (c) Membrane 1.4 (30 % $NaHCO_3$) and (d) Membrane 2.1 (20 % water, spin-coated at 500 rpm). Red and blue denote the large pore and small pores respectively within the membrane. Scale bars represent 200 µm.*

In addition, the release of CO_2 may also be responsible for the formation of through-channels in the PDMS membranes, which could explain the occurrence of leakages observed in membrane 1.9.

The formation of through-channels in the membranes is a non-desirable phenomenon for our application since the goal is to achieve a leakage-free hydrophobic membrane with increased permeability to oxygen gas. However, if the diameter of the channels that form are sufficiently small, they do not pose a great risk of leakage due to a capillary action effect in which the combination of surface tension (caused by the cohesion within the liquid) and adhesive forces between the liquid and channel walls act to keep the liquid from passing through the membrane. Comparing the membranes developed using embedded $NaHCO_3$ particles at different concentrations with the membrane developed by water-in-PDMS emulsion (Figure 3.1 – (d)), it is evident that the latter reveal much smaller pore-sizes. Since pore sizes of the microporous membranes (2.1 to 2.3) were significantly

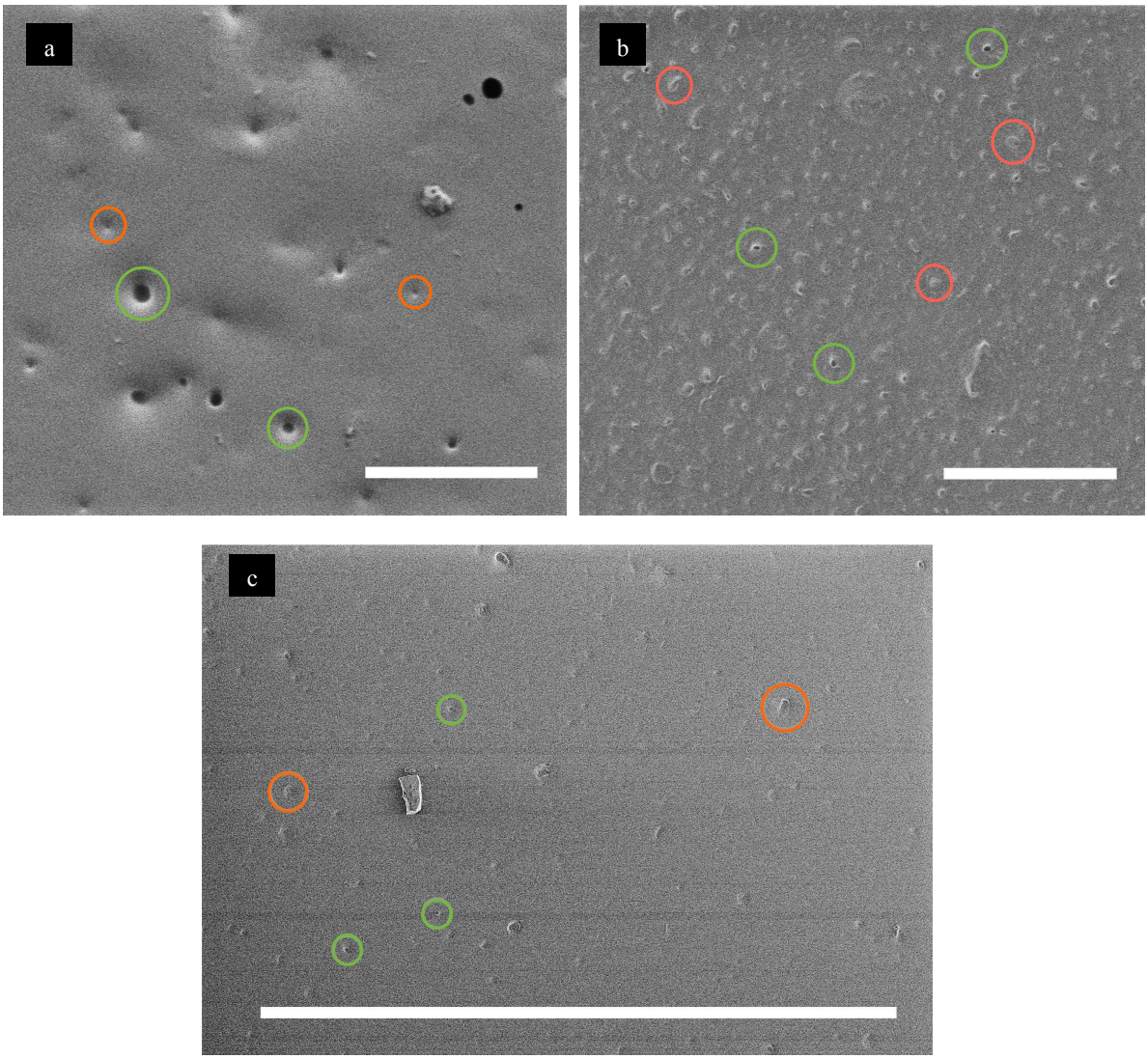

Figure 3.2. *SEM images of the prepared microporous PDMS membranes. (a) Membrane 2.1 (20 % water, spin-coated at 500 rpm); (b) Membrane 2.3 (30 % water, spin-coated at 1000 rpm) and (c) Membrane 2.2 (20 % water, spin-coated at 1000 rpm). Green and orange represent holes and cavities respectively on the membrane surface. Scale bars represent 50 µm.*

smaller and not clearly visibly by light microscopy, they were imaged under SEM, depicted in Figure 3.2. The green circles outline holes while the orange circles outline cavities formed on the surface of the membranes as a result of the evaporation of the trapped water bubbles within the membranes. The difference between these two formations on the surface is simply due to the different position of the trapped water bubbles in the partially cured PDMS. Water bubbles that were trapped near the surface of the membrane resulted in cavities while the water bubbles that were trapped further in the membrane network resulted in holes. Here, unlike in the $NaHCO_3$-based membranes, there is little to no chance of through-channel formation, but rather dead-ended tunnels. These membranes revealed pore sizes ranging between 0.4 and 2 µm. However, differences regarding pore sizes as well as cavity/hole formation are observed between the membranes spin-coated at different speeds (500 and 1000 rpm). The SEM results show that membranes spin-coated at a 1000 rpm (Figure 3.2 – (b) and

(c)) revealed significantly smaller pore sizes and a larger number of cavities (rather than holes) on the membrane surface in comparison to the membrane spin-coated at 500 rpm (Figure 3.2 – (a)). This suggests that at higher rotational speeds, the droplets were found closer to the surface of the membrane, which may be explained by the thinning of the membrane (as the film thins, its surface passes through several cross-sections of more particles than a thicker film would). The smaller pore sizes for the membranes developed at 1000 rpm occur as a result of the larger water droplets (with a higher mass) being spun off the edge of the substrate due to the higher centrifugal force. In other words, the higher rotational speeds promote a selective removal of water droplets with higher mass, leaving behind the smaller water droplets. In addition, it is evident that higher concentrations of pores are visible in the membrane developed using a higher concentration of water droplets.

In our application, the main goal is to achieve a membrane with the highest O_2 permeability possible, while still maintaining integrity and uniformity of the membrane in order to avoid the formation of O_2 bubbles and leakages. The water-in-PDMS technique enabled simple development of microporous PDMS membranes with much higher uniformity while still providing a significant number of pores, compared to the membranes developed using $NaHCO_3$ particles. This method showed to be much more practical since there is no need to soak the membranes for several hours/days in order to wash away the porogen particles.

The porosities of the developed PDMS membranes were quantified by image analysis and are represented in Table 3.3.

Table 3.3. *Porosity of the macroporous and microporous PDMS membranes.*

	$NaHCO_3$ (%)			**Water (%)**		
	10	20	30	20		30
Spin-coating speed	500	500	500	500	1000	1000
Porosity, *n* (%)	34	54	85	18	25	33

For the macroporous membranes, developed using $NaHCO_3$, results show that the porosity of the membranes depends on the percentage of $NaHCO_3$ particles embedded in PDMS. Higher amounts of $NaHCO_3$ particles result in membranes with higher porosities. The highest percent porosity (85 %) was achieved for the membrane developed using 30 % $NaHCO_3$.

Regarding the membranes developed by water-in-PDMS emulsion, the same trend was verified in which an increased percentage in water resulted in membranes with increased porosity. The highest porosity (33 %) was achieved for the membrane developed by 30 % water-in-PDMS. In addition, this data reveals a slight increase in porosity for the 20 % water-in-PDMS membrane, spin-coated at 1000 rpm compared to the 20 % water-in-PDMS membrane, spin-coated at 500 rpm, which means that spin-coating at higher rotational speeds does not compromise the porosity values of the membranes. With the latter in consideration, it is possible to develop thinner microporous PDMS membranes with approximately the same porosity, and therefore greatly increase the overall membrane permeability to

oxygen. Even though in eq. 1.3, the permeability is normalized by thickness, the amount of gas that diffuses through the membrane does depend on the thickness, meaning that thinner membranes result in more total gas diffusion.

The possibility of achieving a higher porosity using this technique whilst maintaining the current thicknesses (70 – 200 μm) revealed itself challenging given the difficulty encountered when mixing higher quantities (> 30 %) of water in PDMS by manual blending. In order to do so, mechanical blending may be required.

3.1.1 Membrane Permeability Measurements

The permeation properties were determined utilizing a constant flow-rate/variable pressure apparatus with known membrane thicknesses and a known exposed membrane surface area (12.5 mm^2). Permeability measurements were solely carried out for the microporous PDMS membranes, namely the membranes developed by 20 and 30 % water-in-PDMS emulsion. A standard non-porous PDMS membrane was initially tested on the membrane for comparison. According to eq. 1.3, we were able to calculate the permeabilities of the membranes, with known thickness and exposed surface area, by applying a constant known flow-rate and measuring the pressure in the chamber once the system is stabilized. Table 3.4 shows the oxygen permeability values for the membranes, determined using the permeation-measuring apparatus.

Table 3.4. *Measured O_2 permeability of the developed membranes.*

Membranes	**Permeability to O_2 $\times 10^9$** $[cm^3\ (RTP)\ \cdot\ cm\ \cdot\ s^{-1}\ \cdot\ cm^{-2}\ \cdot\ cm\ Hg^{-1}]$
Non-porous PDMS	78
Microporous PDMS, 20 % water	129
Microporous PDMS, 30 % water	175

For the standard non-porous PDMS membrane, a permeability value of 78×10^9 $[cm^3\ (RTP) \cdot\ cm \cdot s^{-1} \cdot cm^{-2} \cdot cm\ Hg^{-1}]$ was obtained. The proximity of this value with the value of standard PDMS permeability, measured under similar conditions, found in literature (60×10^9 $[cm^3\ (RTP) \cdot\ cm \cdot s^{-1} \cdot cm^{-2} \cdot cm\ Hg^{-1}]$) [18], indicates that the setup we developed represents a viable and practical methodology of determining polymeric membrane permeabilities in a laboratory setting.

In comparison to the non-porous PDMS, both microporous PDMS membranes revealed higher permeability values: 129×10^9 $[cm^3\ (RTP) \cdot\ cm \cdot s^{-1} \cdot cm^{-2} \cdot cm\ Hg^{-1}]$ and 175×10^9 $[cm^3\ (RTP) \cdot\ cm \cdot s^{-1} \cdot cm^{-2} \cdot cm\ Hg^{-1}]$ for the membranes made with 20 % and 30 % water-in-PDMS respectively. This confirms that the presence of pores in the PDMS membrane structure significantly increases the permeability of the membranes.

3.1.2 Membrane Expansion test

A standard non-porous PDMS membrane was tested in regard to its deflection capacity in order to determine the approximate amount of pressure PDMS membranes are able withstand without tearing. Figure 3.3 shows several images of the membrane taken for increasing pressure differences.

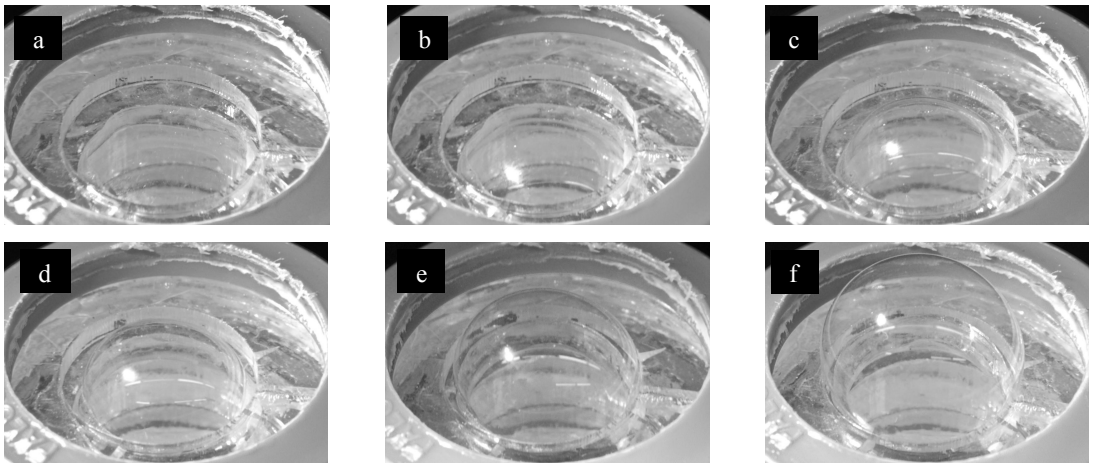

Figure 3.3. *Expansion of PDMS membrane with increasing pressures. P = Pressure applied inside platform. (a) P = 20 mm Hg; (b) P = 120 mm Hg; (c) P = 220 mm Hg; (d) P = 420 mm Hg; (e) P = 630 mm Hg and (f) P = 820 mm Hg.*

It is visually evident that the membrane deflection increases with increasing pressures inside the chamber from 10 mm Hg to 820 mm Hg. The maximum applicable pressure by the 60 mL syringe was 820 mmHg. Even at this pressure, there were no visible signs of rupture, tear or leakage of the membrane. The elasticity of the PDMS membrane allows significant deflection to occur when a pressure difference develops. This property provides the potential to enlarge the diffusion area as the membrane extends, which in turn increases the final oxygen permeation rate. According to these measurements, a standard non-porous PDMS membrane is able to withstand pressures higher than 820 mm Hg. For this approach, applying a certain amount of pressure to the device (and in future to the engineered catheter) will allow a safe amount of deflection of the material, which will not only decrease the materials thickness but also increase the surface areas. These two factors play a vital role in increasing the oxygen permeation rate through the membrane, into the circulating medium (water for testing and blood in the real-life application).

3.2 Proof of concept device data

Figure 3.4 depicts the side-view and front-view of the final bench-top testing device used to experimentally evaluate the viability of the suggested approach, consisting of an intravenous catheter for directly supplying sustainable oxygen amounts into the bloodstream. All functional macroporous and microporous PDMS membranes were tested except for membrane 2.3 (30 % water-in-PDMS), which will be tested in future work. Once a membrane is mounted in place on the device, a constant water flow (at 1 mL/min) enters the upper channel and a flow of H_2O_2 (varying between 0.5 and 2.5 mL/min) enters the lower channel in the opposing direction.

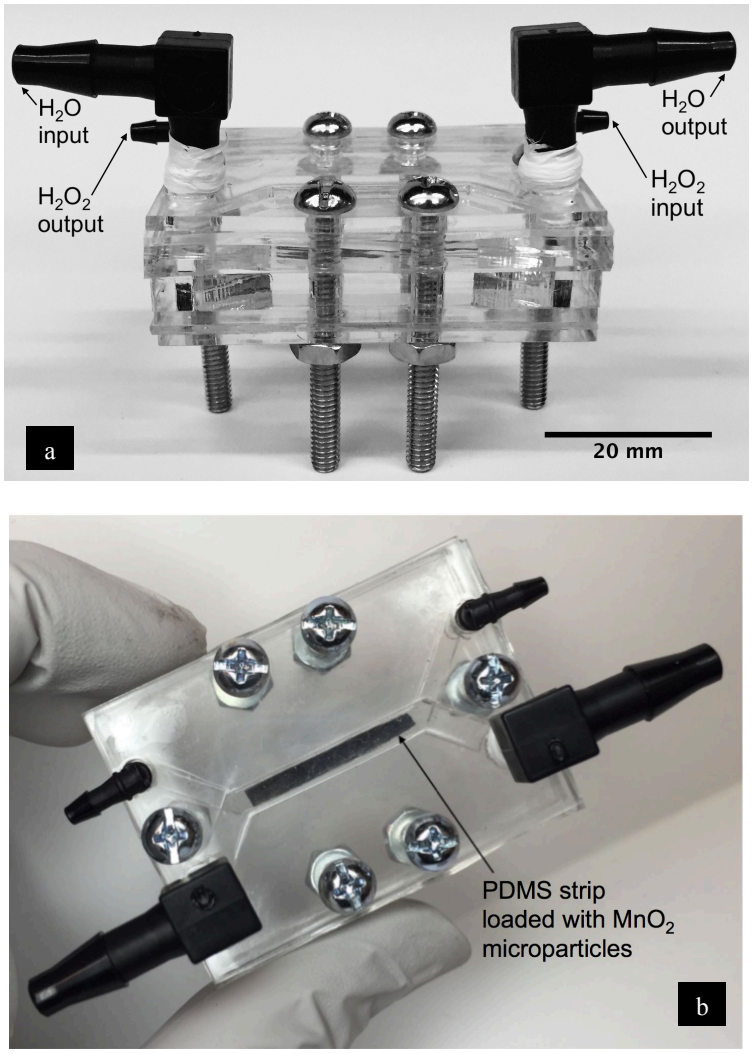

Figure 3.4. *Pictures of the fabricated test device. (a) Side view, indicating the water and hydrogen peroxide inlets and outlets; (b) top-view.*

Oxygen was immediately generated by catalytic decomposition of H_2O_2 once it reached the MnO_2 microparticles within the channel. While the hydrostatic pressure in the upper channel was kept constant at 10 mm Hg, the increasing pressures in the lower channel increased the pressure difference across the membrane.

Since the initial concentration of oxygen in the deoxygenated water (bubbled in Nitrogen gas) is approximately zero, the partial pressure in the first instances is also zero and increases as the oxygen concentration in the water increases. The oxygen concentration in the water channel resulting from the permeation from the H_2O_2 channel, through the exposed membrane area (A = 60 mm^2), is measured in ppm (1 ppm = 0.001 mL/L) by an O_2 sensor. Knowing that the flow-rate in the water channel remains constant (at 1 mL/min), we are able to simply convert the measured concentration values into a rate (i.e. the O_2 permeation/transport rate in cm^3/s) accordingly:

$$\frac{\boldsymbol{a}\ mL}{L} \times \frac{0.001\ L}{min} = \frac{\boldsymbol{a}\ mL}{min} = 0.0167\boldsymbol{a}\ cm^3/s$$

The following graphs (see next page) represent the corresponding oxygen permeation rate in the water channel with an increasing pressure difference across the developed macroporous membranes (membranes 1.1 to 1.4 – Table 3.1), plotted in Figure 3.5, and microporous membranes (membranes 2.1 and 2.2 – Table 3.2) [b], plotted in Figure 3.6. Overall, the data show a strong positive correlation between oxygen permeation rates through the membranes and increasing pressure gradient across them. In eq. 1.3, the value of permeability does not depend on the pressure but is normalized by pressure. However, the amount of gas, which diffuses through membrane, does depend on the pressure: a higher pressure differential equates to more gas diffusing through the membrane.

From the membranes developed with varying percentages (0, 10, 20 and 30 %) of embedded $NaHCO_3$, the membrane with the highest $NaHCO_3$ (30 %) revealed the highest oxygen permeation rate of 3.4×10^{-8} cm^3/s into the water channel at the maximum applied ΔP of 16 mm Hg. This can be explained by the increased number of open-spaces within the membrane in comparison to the rest, which was previously verified by light microscopy and porosity analysis of the membranes in section 3.1. Since the diffusion (one of the three permeation mechanisms) of gas molecules in a PDMS membrane is a process in which the molecules migrate from "holes" (free volumes) to "holes" (free volumes), the higher the number of "holes"/voids within the membrane, the higher the permeation rate of oxygen will be. The membrane developed using 10 % $NaHCO_3$ reveled an initial oxygen permeation rate lower than the membrane developed with 0 % $NaHCO_3$, and at ΔP between 7 and 11.5 mm Hg it rose significantly, achieving an oxygen permeation rate higher than the membrane developed with 20 % $NaHCO_3$. This behaviour may have occurred given the non-uniformity of the membrane that could have initially limited the permeation of oxygen as well as the possible presence of a through-channel, resulting from the CO_2 gas release during its development, which may have expanded with increasing pressures, and therefore, caused the observed sudden increase in oxygen permeation.

Regarding the oxygen permeation rates observed for the tested membranes developed by water-in-PDMS emulsion, the membrane that achieved the highest oxygen permeation rate, of 7.2×10^{-8} cm^3/s, was the 70 μm-thick membrane, developed using 20 % water-in-PDMS at a maximum ΔP of 75 mm Hg. Higher pressures were applied for the microporous membrane tests since these showed higher resistance and flexibility compared to the macroporous membranes, that after a certain ΔP (approximately 20 mm Hg) would result in expansion and tearing of the membrane and consequent release of oxygen bubbles into the water channel. Even though the $NaHCO_3$ macroporous membranes with higher PDMS base-crosslinker ratios showed to have a significantly higher porosity compared to the water-in-PDMS microporous membranes, the latter enabled the permeation of increased amounts of oxygen into the water channel.

[b] Membrane 2.3 (see Table 3.2 for details) was not tested on the testing device since it was fabricated following the tests, solely for the permeability measurements in section 3.3.

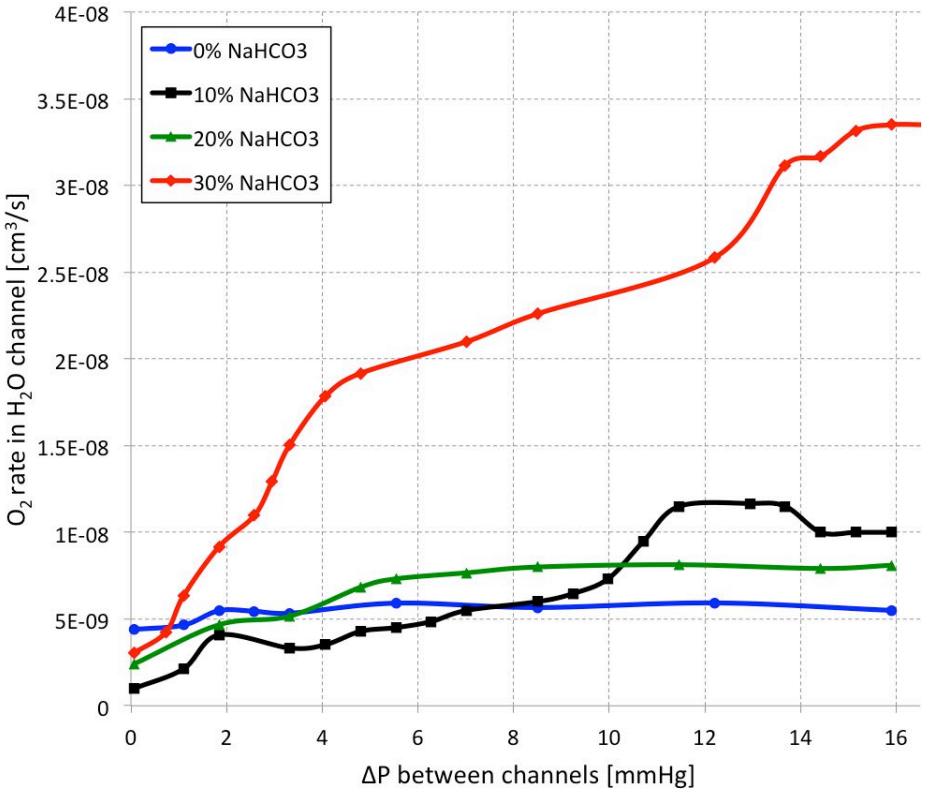

Figure 3.5. *Oxygen permeation/transport rate in the H_2O channel with increasing H_2O_2 channel pressure for the macroporous PDMS membranes.*

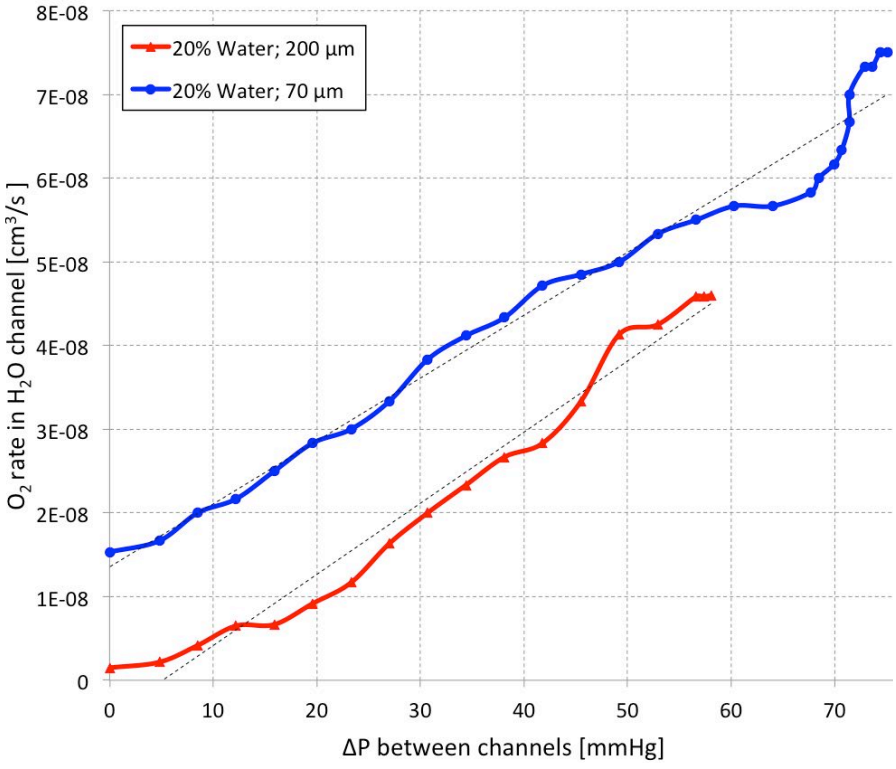

Figure 3.6. *Oxygen permeation/transport rate in the H_2O channel with increasing H_2O_2 channel pressure for the microporous PDMS membranes.*

This is simply due to the lower pressure gradient range applied to the $NaHCO_3$-based membranes and also given the fact they were relatively thicker than the water-in-PDMS-based membranes considering their brittleness otherwise. The dependence on membrane thickness is evident by comparing the two microporous membrane permeation rates, since the only varying parameter between them is indeed the thickness.

As mentioned, the maximum overall oxygen permeation result in water achieved by our device, considering a membrane surface area of 60 mm^2, was 7.2×10^{-8} cm^3 O_2 per second. In order to compare this value to the minimum required oxygen permeation rate (1.6 cm^3/s) to temporarily sustain a patient with only 30 % of their lungs functional, it is first necessary to convert the obtained water data into the equivalent blood data. The equivalent blood data was determined by multiplying the water data by a factor of 5, similarly to what was done by Vaslef et al. [14] and confirmed by Hattler et al. [1]. The main contributing factors to the oxygen permeation differences between water and blood are the different viscosity and oxygen solubility. Accordingly, the equivalent oxygen permeation rate in blood was 3.6×10^{-7} cm^3/s, once again, considering 60 mm^2 of membrane surface area.

For an accurate assessment of the suggested approach viability, it is also necessary to extrapolate the equivalent maximum oxygen permeation value achieved by the device and membrane (3.6×10^{-7} cm^3/s) to the conditions of the practical approach, i.e. surface area of an intravenous catheter and increased pressure gradients. Figure 3.7 shows an extrapolation of the equivalent oxygen permeation rate in blood for various surface areas and pressure differences, taking into account that both parameters are directly proportional to the oxygen permeation rate.

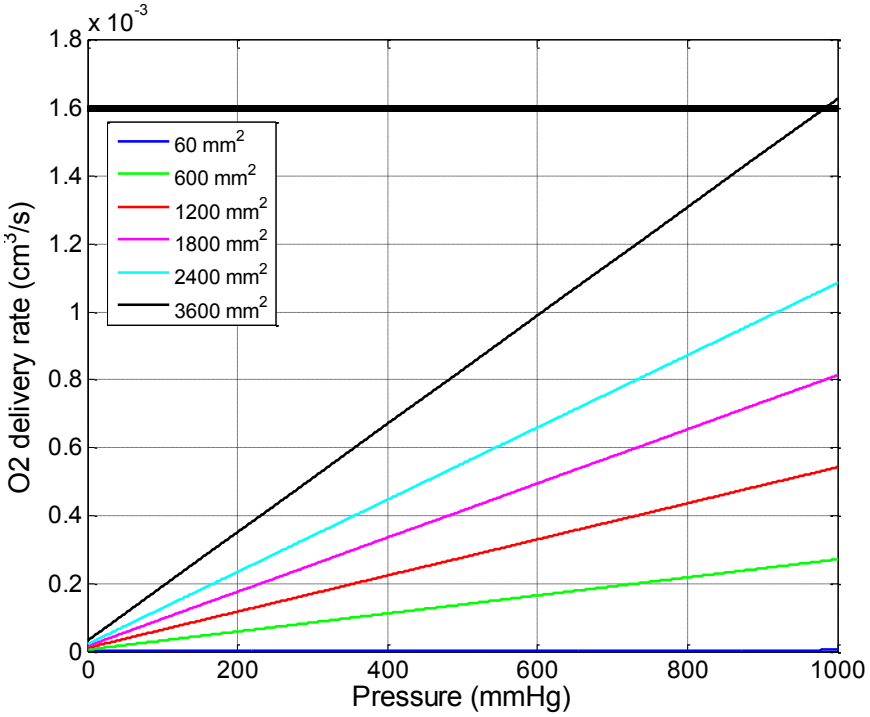

Figure 3.7. *Extrapolation of the maximum oxygen permeation value achieved for increased surface areas and pressure gradients, as an approximation to the real-life application.*

Note that this extrapolation was realized for the membrane that enabled highest oxygen permeation rate into the water channel, namely (20 % Water-in-PDMS, spin-coated at 1000 rpm). The bar outlined at $1.6x10^{-3}$ cm^3/s represents a value that is precisely three orders of magnitude lower than the minimum required oxygen value ($1.6x10$ cm^3/s).

By analyzing the extrapolation, it is evident that by further increasing surface area through which the oxygen permeates as well as the pressure gradient across the membrane, it is possible to significantly increase he oxygen permeation rate through the membrane/catheter material. For the current surface area (60 mm^2) and pressure gradient (75 mm Hg) the proof-of-concept device enables, the oxygen permeation values are minimal compared to what can be achieved using larger surface areas and pressures. For example, and according to what the graph in figure 3.7 represents, for a surface area of 3600 mm^2 (achievable using a 23 cm long catheter with 4 mm diameter) and a pressure gradient of 980 mm Hg, it is possible to achieve a predicted oxygen permeation rate of approximately 1.6×10^{-3} cm^3/s. This result is five orders of magnitude higher than the value achieved by our device but still three orders of magnitude away from the minimum required value.

Although the values shown here do not yet reach the minimum sustainable oxygen permeation rate of 1.6 cm^3/s for temporary whole body oxygenation of a patient diagnosed with acute respiratory failure, there is still room for scaling up the oxygen generation rate. While further increasing and enhancing membrane/material permeability to oxygen is still possible to a certain extent, it is also possible to engineer a catheter with increased surface area that is able to withstand higher pressures, that will altogether contribute to the development of a viable life-sustaining oxygenating system. However, it is still important to note that, the amount of oxygen supply achieved so far, may already be sufficient to aid the oxygenation of specific vital organs (i.e. during surgery or in other hypoxic medical conditions) rather than whole-body oxygenation.

3.3 Polyimide tube with embedded MnO_2 nanoparticles

Carbonization by laser ablation of select regions of a polyimide tube surface was done using a 10.6 μm CO_2 laser in a rectangular pattern, producing blind rectangular regions with 2 mm length and 0.5 mm width. Figure 3.8 shows the carbonized regions on the polyimide tube. A close examination of the carbonized regions show pieces of ablation products randomly protruding from the ablated surface making it rough and therefore increasing surface area significantly. This increased surface area enables MnO_2 nanoparticles, chemically synthesized *in situ* according to eq. 2.1, to be embedded within these regions. Figure 3.8 (b) depicts the generation of oxygen gas bubbles as a result of the catalytic decomposition of 15 % H_2O_2 by the embedded MnO_2 nanoparticles, according to eq. 1.2.

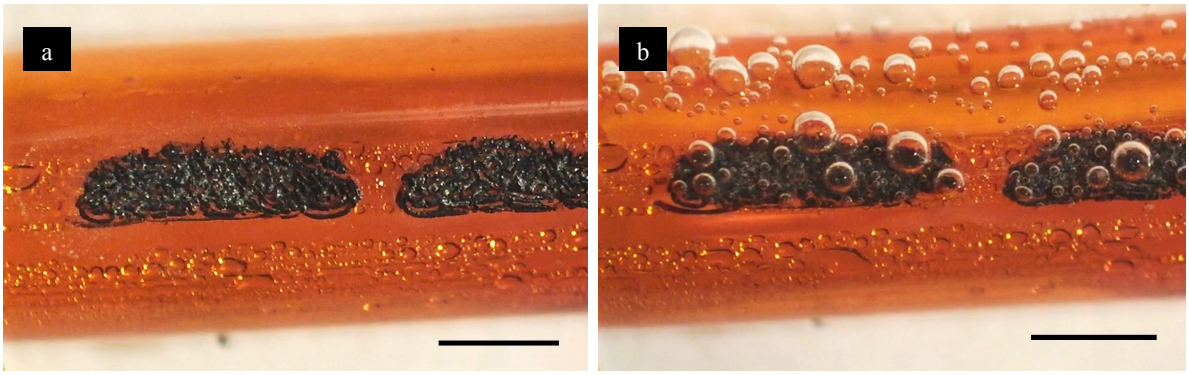

Figure 3.8. *(a) Polyimide tube with select laser ablated regions with embedded MnO_2 particles; (b) Oxygen generation after a droplet of H_2O_2 (30 %) is placed on the surface. with embedded MnO_2 nanoparticles; Scale bar represents 1 mm.*

The generation of oxygen continued for over 5 minutes, with a single 1 mL droplet of 15 % H_2O_2. However, with a constant flow of H_2O_2, as the practical approach suggests, the generation of oxygen would continue for as long as the MnO_2 nanoparticles remain in place.

With the abundant amount of oxygen generated, this methodology has proved to be a promising, unique and straightforward one for the final application, where the generated oxygen would diffuse through the oxygen-permeable PDMS catheter into the bloodstream. Since a crucial factor to the suggested approach is portability, this method of oxygen storage and generation reveals itself as an effective substitute for an oxygen tank, the conventional oxygen storage vessel.

CHAPTER 4. CONCLUSIONS AND FUTURE PERSPECTIVES

4.1 Conclusions

Progress has been made towards developing a straightforward, portable, low cost, and scalable approach for delivering oxygen directly into the bloodstream without the risk of forming oxygen bubbles or hemolysis. The approach, consisting of an intravenous catalytic oxygen-generating catheter, was assessed using a custom-made testing device to mimic the catheter-blood interface, with the aim of achieving a predicted value (extrapolated from the device) corresponding to the minimum oxygen delivery requirements (1.6 cm^3/s) to temporarily sustain a patient suffering from acute respiratory failure with only 30 % of their lungs functional.

The testing device consisted of an oxygen-generating channel ("catheter") and a water channel ("bloodstream") separated from eachother by fabricated porous PDMS membranes for enhanced oxygen-permeability that mimics the catheter material. This device assessed the several membranes that were developed according to the oxygen permeation rate they allow from the "catheter" channel into the "bloodstream" channel.

From the different techniques used in this work to develop the porous PDMS membranes, the combination of increased PDMS base-crosslinker ratios and embedded $NaHCO_3$ particle techniques originated non-uniform macroporous PDMS membranes with pore sizes ranging between 20 and 250 μm. Different porosities were obtained for varying amounts (0, 10, 20 and 30 %) of embedded $NaHCO_3$ particles and the membrane developed using 30 % $NaHCO_3$ particles represented the highest porosity. When assessing these membranes on the testing device, it was verified that the membrane with increased porosity (30 % $NaHCO_3$) also enabled the highest oxygen permeation rate out of all membranes developed using $NaHCO_3$.

On the other hand, the water-in-PDMS emulsion technique enabled the development of microporous PDMS membranes that, to our knowledge, has not yet been accomplished (in membrane form) using this method. Here, the resulting membranes were much more uniform with pore sizes ranging between 0.4 and 2 μm and permeation measurements of these membranes confirmed an increase in oxygen permeability compared to a standard non-porous PDMS membrane. This technique revealed itself as a more practical and feasible one for producing porous PDMS membranes with enhanced permeability, which also enabled the highest overall oxygen permeation rates tested on the device. Despite their higher porosity, the membranes developed by $NaHCO_3$ particle embedment may not be good candidates for being used in the final device as the catheter material, due to: 1. the brittle and stickiness they showed below certain thicknesses; 2. the non-uniformity and 3. the unpredictable formation of through-channels, which could increase the overall risk of oxygen bubble formation.

Another section of this work included the assessment of the suggested oxygen generating technique within the catheter, consisting of a catalytic decomposition of hydrogen peroxide into

oxygen. This proved to be a promising and straightforward oxygen storage and generation method, mainly given its incredible portability compared to the conventionally used oxygen tanks.

In sum, the maximum oxygen permeation rate that was achieved on our device, with a permeation area of 60 mm^2, was 7.2×10^{-8} cm^3/s in water and was obtained for the microporous membrane developed using 20 % water-in-PDMS. The converted permeation rate from water to blood data was 3.6×10^{-7} cm^3/s. The extrapolation of this value to a system with higher surface areas and increased pressure gradients (i.e. in the case of an intravenous catheter), suggested that it is possible to achieve an oxygen permeation rate of approximately 1.6×10^{-3} cm^3/s with a surface area of 3600 mm^2 and ΔP of 980 mm Hg.

Although the values achieved so far are distant from the minimum life-sustaining oxygen permeation rate of 1.6 cm^3/s for temporary whole body oxygenation, they may be scaled further by engineering a smart catheter with increased surface area and optimized membrane permeability. Increasing the pressure and decreasing membrane thickness are also feasible options to increase oxygen permeation rate, although they have higher limitations. In addition, the use of such smart membrane materials renders this approach ideal for mass fabrication via modern nano-manufacturing technologies.

Alternatively, this approach may also be used for local or specific organ oxygenation rather than whole body oxygenation since the oxygen requirements at this level are significantly lower and therefore easily reachable.

4.2 Future work

Apart from the need of further optimization and testing of the oxygen-permeable membranes, future work should focus on engineering a custom catheter with increased surface area, possibly using micron-scale structures throughout the surface. These microstructures can be made using various techniques. One way would be to raster the catheter to roughen it (the roughness would be a micropattern). Another would be to create a wrap-around mold (i.e. sheet with micro holes), which is attached to the catheter temporarily, and then PDMS is screen-printed on; after curing, the mold is removed to reveal PDMS hairs. Another way could be for commercial manufacturing: make catheters using a molding technique with a mold with specific micro-patterns. All the patterns can be defined by standard photolithography techniques or by laser machining.

The inclusion of microstructures on the catheter surface may be a feasible approach to significantly increase oxygen permeation rates through the catheter material, given its proportional increase with overall surface area. For example, considering a 20 cm long catheter with 0.4 cm in diameter, engineered with part of its surface area covered in hollow microstructures (0.5 mm length and 25 μm diameter) as represented in Figure 4.1, the calculated total surface area can be easily scaled up to approximately 2000 cm^2 (200.000 mm^2), as shown in Appendix C.

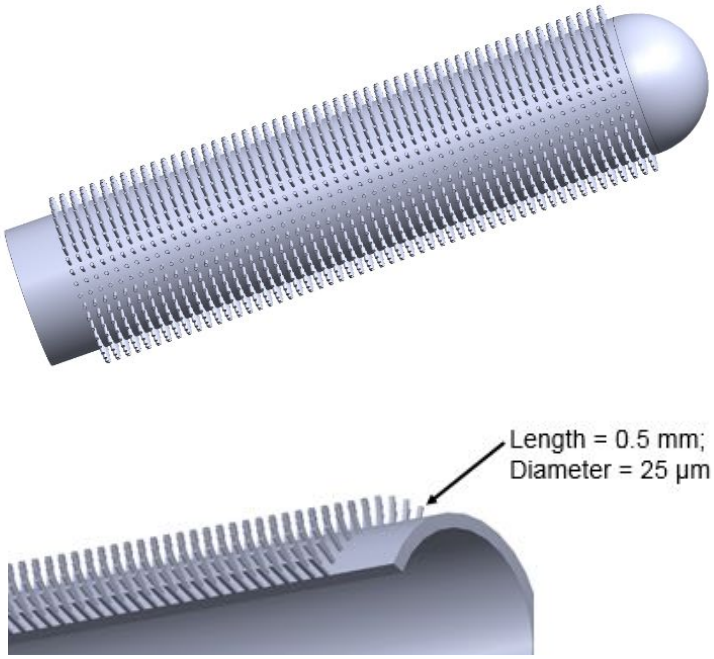

Figure 4.1. *Theoretical approach for an engineered PDMS-based catheter with increased surface area using microstructures.*

By doing this, and considering an applied pressure within the catheter of 820 mm Hg, the predicted oxygen permeation rate would reach 0.012 cm^3/s. The prediction of this value shows that, with some extra tuning of certain parameters such as surface area, thickness, membrane permeability and applied pressure, we are able to achieve promising O_2 permeation values that could one day be sufficient to sustain a human life. Once the suggested approach is achieved and sustainable oxygen permeation values are reached, the oxygen-generating microsystem will have to undergo several clinical trials.

This work was presented in both oral and poster forms at the "NAPA Institute 2015 Workshop on Enabling Future Health Care: the Role of Micro and Nano Technologies" held in Napa, California, USA.

REFERENCES

[1] B. G. Hattler, L. W. Lund, J. Golob, H. Russian, M. F.Lann, T. L. Merrill, B. Frankowski, W. J. Federspiel, "A respiratory gas exchange catheter: in vitro and in vivo tests in large animals", *Journal of Thorac Cardiovascular Surgery*, Sep;124(3):520-30, 2002.

[2] *BMJ Publishing Group, Acute Respiratory Failure*, 2015. [Available online]: bestpractice.bmj.com.

[3] Wilson, Robert F., and William J. Sibbald. "Acute respiratory failure", *Critical Care Medicine*, 4, 79-89, 1976.

[4] *Acute Respiratory Failure*, Healthline Networks, Inc., 2015. [Available online]: www.healthline.com.

[5] M. Kwan, J. Woo and T. Kwok, "The standard oxygen consumption value equivalent to one metabolic equivalent (3.5 mL/min/kg) is not appropriate for elderly people", *International Journal of Food Sciences and Nutrition*, 55, 3, 179-182, 2004.

[6] J. N. Kheir et al., "Oxygen Gas-Filled Microparticles Provide Intravenous Oxygen Delivery" *Science Translational Medicine*, 4, 140, 140ra88–140ra88, 2012.

[7] I. Singh, "Intravenous Injection of Oxygen with the Animal under Ordinary and Increased Atmospheric Pressure", *Journal of Physiology*, 84, 3, 315–322, 1935.

[8] C. L. Stanfield, W.J. Germann, "*Principles of Human Physiology*", Chapter 17: Respiratory System: Gas Exchange and Regulation of Breathing, Pearson Publishing, 2008.

[9] A. Carreau, B. El Hafny-Rahbi, A. Matejuk, C. Grillon C, C. Kieda, "Why is the partial oxygen pressure of human tissues a crucial parameter? Small molecules and hypoxia", *Journal of cellular and molecular medicine*, (6):1239-53., 2011.

[10] R. L. Riley, A. Cournand, "Analysis of Factors Affecting Partial Pressures of Oxygen and Carbon Dioxide in Gas and Blood of Lungs: Theory", *Journal of Applied Physiology*, Vol. 4 no. 2, 77-101, 1951.

[11] K. R. Ward, G. S. Huvard, M. McHugh, R. R. Mallepally, R. Imbruce, "Chemical Oxygen Generation" *Respiratory Care*, 58, no.1, 2013.

[12] B. Z. Shakhashiri, *"Chemical Demonstrations, A Handbook for Teachers of Chemistry",* Wisconsin, Vol.2, p.137-141, 1989.

[13] C. Zheng, "*Nanofabrication – Principles, Capabilities and Limits*", Chapter 5: Nanofabrication by Replication, Springer, 2008.

[14] *Introduction to PDMS: A review*, 2015. [Available online]: http://www.elveflow.com/

[15] A. Lamberti, S. L. Marassoab and M. Cocuzzaab, "PDMS membranes with tunable gas permeability for microfluidic applications", *Royal Society of Chemistry Advances*, 4, 61415, 2014.

[16] K. Jiao, C. L. Graham, J. Wolff, R. G. Iyer, P. Kohli, "Modulating molecular and nanoparticle transport in flexible polydimethylsiloxane membranes", *Journal of Membrane Science*, Elsevier, 2012.

[17] J. Wang, M. Zheng, W. Wang, and Z. Li, "*Chips and Tips*", Royal Society of Chemistry Advances, 1–6, 2014.

[18] W.L. Robb, "Thin silicone membranes--their permeation properties and some applications", *Annals of the New York Academy of Sciences*, 146(1):119-37, 1968.

[19] H. Zhang, "The Permeability Characteristics of Silicone Rubber Haibing Zhang", *Proceedings of 2006 Global Advances in Materials and Process Engineering*, November 6 – 9, 2006, Dallas, TX.

[20] H. B. Tanh Jeazet, C. Staudt, C. Janiak, "A method for increasing permeability in O2/N2 separation with mixed-matrix membranes made of water-stable MIL-101 and polysulfone", 48, *Chemical Communication*., 2012.

[21] S. A. Stern, "The "Barrer" Permeability Unit", *Journal of Polymer Science*, Polymer Physics, Vol 6, Issue 11, pp.1933–1934, 1968.

[22] *Membrane Separation Properties*, 2015. [Available online]: http://www.separationprocesses.com/

[23] K. Berean, J. Z. Ou, M. Nour, K. Latham, C. McSweeney, D. Paull, A. Halim, S. Kentish, C. M. Doherty, A. J. Hill and K. Kalantar-zadeh, "The effect of crosslinking temperature on the permeability of PDMS membranes: Evidence of extraordinary CO2 and CH4 gas permeation", *Separation and Purification Technology Journal*, 122, 96, 2014.

[24] S.N. Vaslef, L.F. Mockros, R.W. Anderson, R.J. Leonard, "Use of a mathematical model to predict oxygen transfer rates in hollow fiber membrane oxygenators", *ASAIO Journal*, 40(4):990-6, 1994.

APPENDIX A

LASER-CUTTER SETTINGS FOR DIFFERENT MATERIALS

Table A.1. *Commercial 10.6 μm CO_2 laser cutter settings for the several materials used.*

Material	Thickness (mm)	Power (%)	Speed (%)	Pulses Per Inch (PPI)	Passes	Mode
Acrylic	5	100	7	1000	1	Vector
Acrylic	1.6	100	10	1000	1	Vector
PDMS	5.5	20	20	1000	5	Vector
Porous PDMS	0.07-0.25	3	3	1000	3	Vector
Polyimide Tube	0.0762*	50	30	750	1	Raster

(*wall thickness)

APPENDIX B

IMAGE OF THE LAB IMPLEMENTATION OF THE TESTING DEVICE

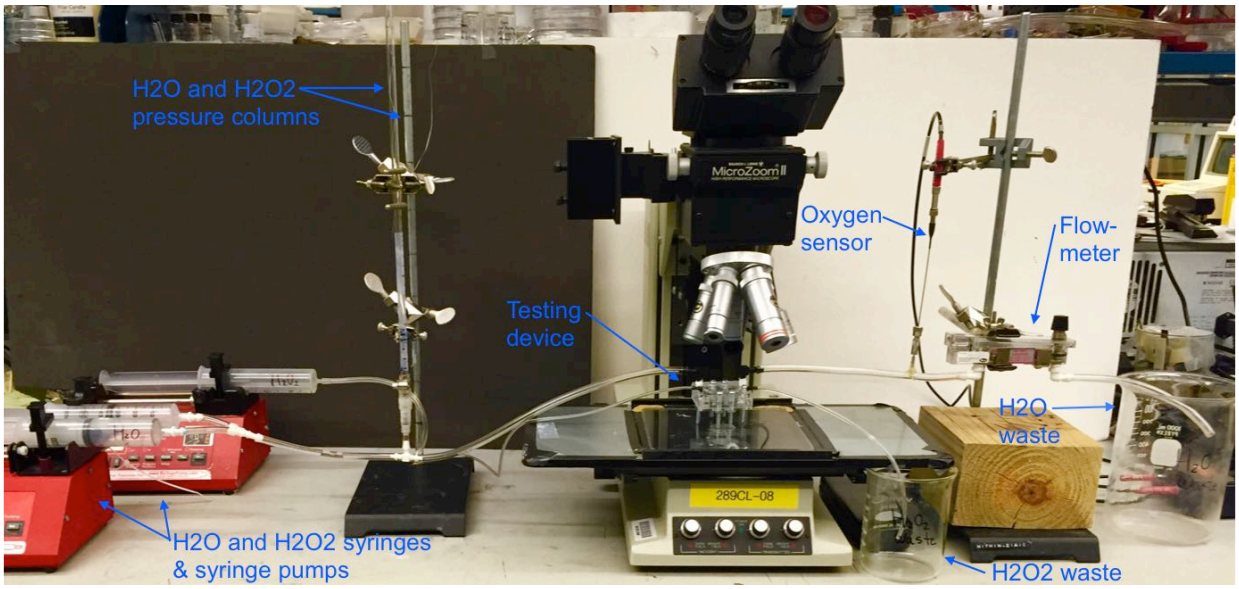

APPENDIX C

CALCULATION OF TOTAL SURFACE AREA OF AN ENGINEERED CUSTOM CATHETER WITH MICROSTRUCTURES

The lateral area (A = 2πrh) of a 20 cm long catheter with 4 mm diameter is approximately 20 cm^2.

Considering that each hollow microstructure is 0.5 mm in length and 20 μm and assuming that 80 % of the catheter is covered in microstructures, the total number of structures on the catheter surface area is:

$$\frac{0.8\times 25\ cm}{\pi r^2} = \frac{0.8 \times 25}{\pi(10\times10^{-4})^2} = 6.4\times10^6\ (6.4\ Million\ microstructures) = N$$

where πr^2 represents the circular area of the catheter surface occupied by each microstructure.
The total surface area of the microstructures is given by:

$$(2\pi rh + \pi r^2) \times N$$

$$=> 2\pi\ (10\times10^{-4})(0.05)\times N + \pi\ (10\times10^{-4})^2\times N = \ 2020\ cm^2$$